Composite Structures 142 (2016) 238–253

Contents lists available at ScienceDirect

Composite Structures

journal homepage: www.elsevier.com/locate/compstruct

Thermal buckling of laminated composite plates using layerwise displacement model

M. Cetkovic *

Faculty of Civil Engineering, University of Belgrade, Bul. Kralja Aleksandra 73, 11000 Belgrade, Serbia

ARTICLE INFO

Article history:
Available online 28 January 2016

Keywords:
Thermal buckling
Layerwise plate theories
Laminates
Analytical solution
Finite element solution

ABSTRACT

In this paper thermal buckling of laminated composite plates, based on Layerwise Theory of Reddy and new version of Layerwise Theory of Reddy, presented for the first time, are formulated using the principle of virtual displacements (PVD). The Navier's analytical solution is derived from the strong form, while the weak form is discretized using the isoparametric finite element approximation. The nine-node Lagrangian isoparametric element is used to derive element stiffness and geometric stiffness matrix. The originally coded MATLAB program is used to investigate the effects of temperature distribution, side to thickness ratio, aspect ratio, modulus ratio E_1/E_2, thermal expansion coefficient ratio α_2/α_1, mesh refinement and boundary conditions on thermal buckling of isotropic, orthotropic and laminated composite plates. The accuracy of the numerical model is verified by comparison with the available results from the literature and some new results are presented.

1. Introduction

Thermal buckling analysis becomes of primary importance for structural components used for high-speed aircrafts, rockets and space vehicles, where thermal loads are induced due to aerodynamic and solar radiation heating, as well as for nuclear reactors or chemical plants, usually subjected to elevated temperature regime during their service life. In such an environment, the temperature differences between the upper and lower surfaces of skin panels often result in large thermal gradients which may lead to excessive deflections and compressive stresses [11]. At certain critical temperature these deflections and stresses may cause the skin panels to buckle. The importance of buckling is the initiation of deflection pattern, which if the temperature is further increases above the critical value, rapidly leads to very large deflections and eventually complete failure of the plate. Hence, the buckling behavior of composite laminates under thermal loads has become the major design criteria for efficient and optimal usage of these materials in structural design. Although considerable literature has been reported to the buckling analysis of laminated composite plates subjected to mechanical load, rather limited investigations analyze thermal buckling problem [9].

One of the earliest studies to examine thermal buckling of plates is that conducted by Gossard et al. [1]. They used Rayleigh–Ritz method to calculate buckling temperature of simply-supported isotropic rectangular plates. Klosner and Furry [2] also used Rayleigh–Ritz procedure to analyze buckling of simply supported plates under different types of temperature distribution. Miura [3] analyzed thermal buckling of plates similar to [2], but with different boundary conditions. Gowda and Pandalai [4] studied thermal buckling of orthotropic plates under uniform and linearly varying temperature distributions. Whitney and Ashton [5] used energy formulation for thermal buckling of symmetric, angle-ply layered composite plates with simply supported edges. Prabhu and Durvasula [6] used Galerkin's method to analyze skew plates under arbitrarily varying temperature distribution.

Generally, mathematical models for thermal buckling analysis of composite laminates have been formulated using three dimensional theory of elasticity (3D), Equivalent Single Layer Theories (ESL), layerwise theories (LW) or Zig-Zag theories. Although the 3D theory of elasticity is a powerful tool for exact analyses of laminated composites with severe variations in the material properties, only restricted solutions have been provided by Noor and Burton [46–48] for thermal buckling problem. The most of the literature regarding thermal buckling problem are based on ESL theories, which are Classical Laminated Plate Theory (CLPT), First-order Shear Deformation Theory (FSDT) and Higher-order Shear Deformation Theory (HSDT).

A thermal buckling solution based on CLPT is firstly given by Jones [7]. Tauchert and Huang [8] used Rayleigh–Ritz technique to analyze the thermal buckling of symmetric angle-ply laminated

* Tel.: +381 11 3218578; fax: +381 11 3370223.
E-mail address: marina@grf.bg.ac.rs

http://dx.doi.org/10.1016/j.compstruct.2016.01.082
0263-8223/

plates based on CLPT. They analyzed plates subjected to a uniform temperature rise and two types of simply supported boundary conditions. Chen and Chen [9] used Galerkin's method to study thermal buckling of laminated cylindrical plates under uniformly distributed temperature filed. They extended their work to include a nonuniform temperature field by using the finite element method (FEM) [10]. Javaheri and Eslami [11] reported thermal buckling of functionally graded plates based on CLPT.

However, the CLPT neglects transverse shear deformation and therefore becomes inadequate for the analysis of moderately thick to thick laminated composites. In this cases, the shear deformation theory or First-order-Shear-Deformation-Theory (FSDT), which assumes constant transverse shear strains, should be adopted [19,21,29]. Tauchert [12] studied the thermal buckling behavior of antisymmetric angle-ply laminates using FSDT. Thangratnam et al. [13] used the FEM to study the thermal buckling of laminated plates based on FSDT. The effects of aspect ratio, moduli ratio, temperature distribution, thermal expansion coefficient ratio and number of layers on buckling temperature were examined. Noor and Burton [14] used predictor–corrector procedures for thermal buckling analysis of laminated composite plates, and compared the results with the analytical three-dimensional thermo elasticity solution. It is shown that the predictor–corrector method delivers very accurate results. Chen et al. [15] used FEM to study thermal buckling behavior of composite laminated plates subjected to uniform or non-uniform temperature fields, based on FSDT. Mathew et al. [16] also used FEM to calculate the buckling temperature of symmetric and asymmetric cross-ply composite beams based on the FSDT. Huang and Tauchert [17] employed FSDT to calculate buckling temperature of clamped symmetric laminated plates. Chen and Liu [18] have given Levy-Type solution for thermal buckling of antisymmetric angle-ply laminates, based on FSDT. Prabhut and Dhanaraj [20] used FEM based on FSDT to calculate thermal buckling load of laminated composite plates. Mannini [22] investigated thermal buckling of symmetric and antisymmetric cross-ply composite laminates, based on FSDT. Kant and Babu [23] employed a shear deformable finite element to study thermal buckling of skew fiber-reinforced composite plates. Singh et al. [24] investigated the thermal post buckling behavior of laminated composite plates by a four-node first-order shear deformable element. Temperature-dependent thermal and elastic properties are used in the analysis. Kabir et al. [25] proposed a first-order shear deformable three-node element for thermal buckling analysis of composite plates. Wu [26] derived equilibrium and stability equations of a moderately thick rectangular plate made of functionally graded materials under thermal loads based on FSDT. Recently, Kabir et al. [27] presented a thermal buckling analysis for perfect, clamped rectangular plates using FSDT. Material properties are assumed to remain unchanged as temperature varies. Finally, Bouazza et al. [28] investigated the thermal buckling of FGM plate using FSDT.

As a result of assumed displacement filed in FSDT, the transverse shear strains are constant through the plate thickness, obtained by the direct constitutive approach and the shear correction factors have to be adopted. However, the shear correction factors are not easy accurately to predict and a Higher-order Shear Deformation Theory (HSDT) should be adopted [70]. The HSDT includes higher-order terms in in-plane displacements and may or may not include higher order terms in transverse direction, which is especially important in thermal environment. Also, unlike FSDT, HSDT are able to satisfy the stress-free boundary conditions and continuity conditions at the interfaces between the layers, by integrating the three-dimensional equilibrium equations [58]. Sun and Hsu [30] indicated that the transverse shear deformation has a significant effect on the thermal buckling behavior of simply supported plates with symmetric cross-ply lamination. Chang [31] preformed FEM analysis of buckling and thermal buckling of antisymmetric clamped angle-ply laminates subjected to in-plane edge loads or uniform temperature rise. The HSDT, including higher-order terms along the transverse direction, was applied through the analysis. Rohwer [33] reported that the result from Chang and Leu [32] have been found to be invalid due to neglecting the stress-free boundary condition at the top and bottom surfaces of a plate. To account for the effect of transverse normal strain on the thermal buckling of laminated composites Chang [34] proposes HSDT solutions. Shu and Sun [35] studied the thermal buckling of cross-ply simply supported plates using HSDT. Shen [36,37] employed a HSDT and von Karman strain–displacement equations for the post buckling analysis of geometrically imperfect composite plates using perturbation method. Kant and Babu [38] employed a shear deformable finite element model to study thermal buckling of skew fiber-reinforced composite plates. Babu and Kant [39] used two refined HSDT that one neglects and the other takes into account the affect of transverse normal deformation to develop two discrete finite element models for the thermal buckling analysis of composite laminates. Dafedar and Desai [40] used HSDT that includes the effects of transverse shear and normal stress for thermo-mechanical buckling analysis of laminated composite plates.

Finally, in wish to unify the order and the type of theories, Carrera proposed so called Carrera's Unified Formulation (CUF), firstly developed for plates and shells, and recently extended to beam models. The CUF removes the inconsistency of generating a large variety of 2D and quasi-3D hierarchical models using unified approach. The unified approach assumes that the variational statement and governing differential equations are written in terms of fundamental nuclei, which are mathematically and formally independent from the expansion orders used in the displacement field and from the kinematic description used such as equivalent single layer or layer-wise [72]. Among other multi field problems, CUF has been implemented on thermal stress problems as well [63,68,72–76]. Results for thermal buckling using CUF are given by Fazzolari [77], as well as by Matsunaga [41,62], who formulated a fundamental set of equations of two-dimensional higher-order plate theory, using power series expansion of displacement components.

At the authors knowledge, not many papers studied thermal buckling using layerwise concept, except Lee and Shariyat [42,43] and two papers [44,45] using local–global or Zig-Zag plate theory [59]. In wish to fulfill the lack of thermal buckling solutions based on layerwise plate theories in the literature, and since limited 3D elasticity solutions are available, in this paper a layerwise finite element and analytical solution for thermal buckling analysis are formulated. After establishing the accuracy of the present layerwise model for linear and geometrically nonlinear bending, vibration and buckling analysis of laminated composite and sandwich plates subjected to mechanical load in the authors previous papers [49,50] as well as for thermal bending of laminated composite and sandwich plates [51], in this paper a thermal buckling analysis is further investigated. In order to take into account amendments of Koiter's recommendation (KR): "a refinement of classical models are meaningless, in general, unless the effects on interlaminar continuous transverse shear and normal stresses are both taken in a multilayered plate/shell theory", as well as Carrera's recommendation [68]: "plate theories with at least a quadratic transverse displacement field in the z direction are required to capture transverse normal strain caused by the linear distribution of temperature across the thickness", in this paper both new variation of LW Theory of Reddy as well as Generalized Layerwise Plate Theory (GLPT) [53] of Reddy are formulated for thermal buckling problem of laminated composite plates. The Present LW Theory, still not reported in the literature, accounts for the layerwise description

of in-plane displacements components and quadratic variation of transverse displacement, thus allowing for the through the thickness deformation. A quasi-static theory of linear thermo-elasticity without coupling between heat conduction and elasticity problem is adopted. The mathematical model assumes layerwise variation of in-plane displacements and constant transverse displacement through the thickness of the plate, non-linear strain–displacement relations (in von Karman sense) and linear thermo mechanical material properties. The governing Euler–Lagrange differential equations, as well as the weak form of linearized buckling problem are derived using principle of virtual displacements (PVD). An Euler–Lagrange differential equations are used to derive Navier's analytical solution, while the weak form is discretized using isoparametric finite element formulation. The original MATLAB program is coded for both analytical and finite element solutions. The effects of temperature distribution, side to thickness ratio, aspect ratio, modulus ratio E_1/E_2, thermal expansion coefficient ratio α_2/α_1, lamination scheme, mesh refinement and boundary conditions on critical temperature of laminated composite plates are analyzed. The accuracy of the numerical model is verified by comparison with the available results from the literature and some new results are also presented.

2. Theoretical formulations of two layerwise plate theories

2.1. Assumptions and geometry of laminated plate

A laminated plate composed of n orthotropic lamina is considered. It is assumed that (1) layers are perfectly bonded together, (2) material of each layer is linearly elastic and has three planes of material symmetry (i.e. orthotropic), (3) strains are small, (4) each layer is of uniform thickness, (5) the extensibility of normal is imposed in the Present LW Theory, while the inextensibility is imposed in LW Theory of Reddy.

2.2. Governing equations of the Present Layerwise Theory

2.2.1. Displacement field

The displacements components (u, v, w) at a point (x, y, z) are expressed as:

$$u(x,y,z) = u_0(x,y) + \sum_{I=1}^{N} U^I(x,y)\cdot\Phi^I(z),$$
$$v(x,y,z) = v_0(x,y) + \sum_{I=1}^{N} V^I(x,y)\cdot\Phi^I(z),$$
$$w(x,y,z) = w_0(x,y) + w_1(x,y)\cdot z + w_2(x,y)\cdot z^2, \quad (1)$$

where (u_0, v_0, w_0) are displacements of a point $(x, y, 0)$ on the reference plane of the laminate, functions $\Phi^I(z)$ are one-dimensional linear Lagrange interpolation functions of thickness coordinates and (U^I, V^I) are the values of (u, v) at the Ith plane, w_1 denote rotation, while w_2 is higher order translation in transverse direction, Fig. 1.

2.2.2. Strain displacement relations

The strains associated with the displacement field (1) are computed using von Karman's non-linear strain–displacement relation:

$$\begin{Bmatrix}\varepsilon_{xx}\\ \varepsilon_{yy}\\ \gamma_{xy}\\ \gamma_{xz}\\ \gamma_{yz}\\ \varepsilon_{zz}\end{Bmatrix} = \begin{Bmatrix}\frac{\partial u}{\partial x}+\frac{1}{2}\left(\frac{\partial w}{\partial x}\right)^2\\ \frac{\partial v}{\partial y}+\frac{1}{2}\left(\frac{\partial w}{\partial y}\right)^2\\ \frac{\partial u}{\partial y}+\frac{\partial v}{\partial y}+\frac{\partial w}{\partial x}\frac{\partial w}{\partial y}\\ \frac{\partial u}{\partial z}+\frac{\partial w}{\partial x}\\ \frac{\partial v}{\partial z}+\frac{\partial w}{\partial y}\\ \frac{\partial w}{\partial z}\end{Bmatrix} = \{\varepsilon_{0L}\}+\{\varepsilon_{NL}\}+z\cdot\{\varepsilon_1\}$$
$$+ z^2\cdot\{\varepsilon_2\} + \sum_{I=1}^{N}\left[\Phi^I\right]\cdot\{\varepsilon_I\}, \quad (2)$$

where:

$$\{\varepsilon_{0L}\}^T = \left\{\frac{\partial u_0}{\partial x}\quad\frac{\partial v_0}{\partial y}\quad\frac{\partial u_0}{\partial y}+\frac{\partial v_0}{\partial x}\quad\frac{\partial w_0}{\partial x}\quad\frac{\partial w_0}{\partial y}\quad w_1\right\},$$
$$\{\varepsilon_{NL}\}^T = \left\{\frac{1}{2}\left(\frac{\partial w}{\partial x}\right)^2\quad\frac{1}{2}\left(\frac{\partial w}{\partial y}\right)^2\quad\frac{\partial w}{\partial x}\frac{\partial w}{\partial y}\quad 0\quad 0\quad 0\right\},$$
$$\{\varepsilon_1\}^T = \left\{0\quad 0\quad 0\quad\frac{\partial w_1}{\partial x}\quad\frac{\partial w_1}{\partial y}\quad 2w_2\right\},$$
$$\{\varepsilon_2\}^T = \left\{0\quad 0\quad 0\quad\frac{\partial w_2}{\partial x}\quad\frac{\partial w_2}{\partial y}\quad 0\right\},$$
$$\{\varepsilon_I\}^T = \left\{\frac{\partial U^I}{\partial x}\quad\frac{\partial V^I}{\partial x}\quad\frac{\partial U^I}{\partial y}+\frac{\partial V^I}{\partial x}\quad U^I\quad V^I\quad 0\right\},$$

$$[\Phi^I] = \begin{bmatrix}\Phi^I & & & & & \\ & \Phi^I & & & & \\ & & \Phi^I & & & \\ & & & \frac{d\Phi^I}{dz} & & \\ & & & & \frac{d\Phi^I}{dz} & \\ & & & & & 0\end{bmatrix}.$$

2.2.3. Constitutive equations

The stress–strain relations for kth orthotropic lamina in global coordinates are given as:

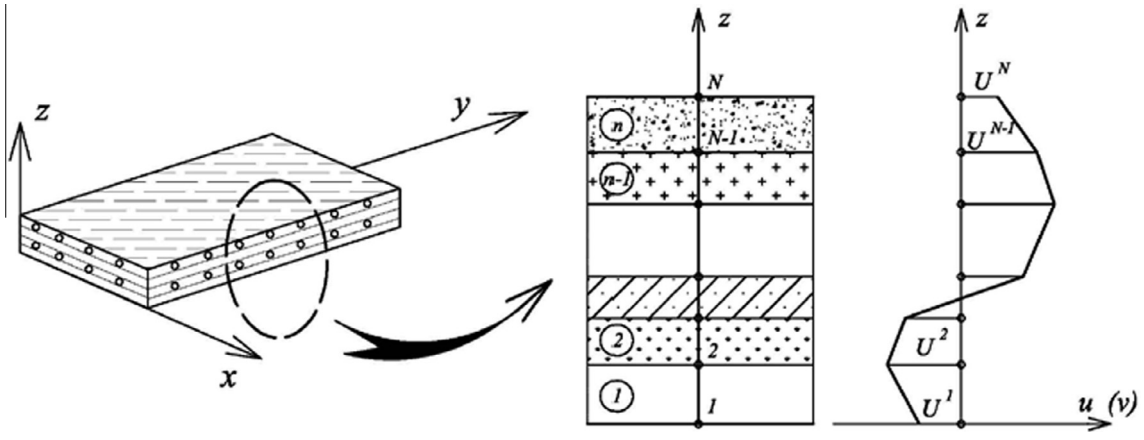

Fig. 1. Multilayer laminated plate.

$$\begin{Bmatrix}\sigma_{xx}\\ \sigma_{yy}\\ \tau_{xy}\\ \tau_{xz}\\ \tau_{yz}\\ \sigma_{zz}\end{Bmatrix}^{(k)} = \begin{bmatrix} Q_{11} & Q_{12} & Q_{13} & 0 & 0 & Q_{16}\\ & Q_{22} & Q_{23} & 0 & 0 & Q_{26}\\ & & Q_{33} & 0 & 0 & Q_{36}\\ & & & Q_{44} & Q_{45} & 0\\ \textit{symmetric} & & & & Q_{55} & 0\\ & & & & & Q_{66}\end{bmatrix}^{(k)} \times \left(\begin{Bmatrix}\varepsilon_{xx}\\ \varepsilon_{yy}\\ \gamma_{xy}\\ \gamma_{xz}\\ \gamma_{yz}\\ \varepsilon_{zz}\end{Bmatrix}^{(k)} - \begin{Bmatrix}\alpha_{xx}\\ \alpha_{yy}\\ \alpha_{xy}\\ 0\\ 0\\ \alpha_{zz}\end{Bmatrix}^{(k)} \cdot \Delta T \right), \tag{3}$$

where $\boldsymbol{\sigma}^{(k)} = \{\sigma_{xx} \;\; \sigma_{yy} \;\; \tau_{xy} \;\; \tau_{xz} \;\; \tau_{yz} \;\; \sigma_{zz}\}^{(k)^T}$ and $\boldsymbol{\varepsilon}^{(k)} = \{\varepsilon_{xx} \;\; \varepsilon_{yy} \;\; \gamma_{xy} \;\; \gamma_{xz} \;\; \gamma_{yz} \;\; \varepsilon_{zz}\}^{(k)^T}$ are stress and strain components, respectively, and $Q_{ij}^{(k)}$ are transformed elastic coefficients, of kth lamina in global coordinates, $\alpha^{(k)} = \{\alpha_{xx} \;\; \alpha_{yy} \;\; \alpha_{xy} \;\; 0 \;\; 0 \;\; \alpha_{zz}\}^{(k)^T}$ are coefficients of thermal expansion, of kth lamina in global coordinates, while ΔT is temperature rise.

2.2.4. Temperature rise

In the present analysis two different temperature distributions are taken into account: the uniform and linear temperature rise.

For the uniform temperature rise the plate initial temperature is assumed to be T_i. The temperature is uniformly raised to final value T_f in which the plate buckles. The temperature change is then:

$$\Delta T = T_f - T_i. \tag{4}$$

The linear temperature rise assumes to vary linearly through the thickness from the top surface temperature T_t to bottom surface temperature and is given as:

$$\Delta T(z) = \frac{\Delta T}{h}\left(z + \frac{h}{2}\right) + T_b, \tag{5}$$

where $\Delta T = T_t - T_b$, while z is the coordinate variable in the thickness direction measured from the middle plane of the plate.

2.2.5. Governing equations and boundary conditions

The governing equations of the Present LW Theory are derived using the principle of virtual displacements (PVD). After performing the integration in the thickness direction the internal work and external work due to in-plane thermal forces become:

$$\delta V + \delta U = \int_\Omega [\{\delta\varepsilon_{0L}\}^T \cdot \{N\} + \{\delta\varepsilon_1\}^T \cdot \{M\} + \{\delta\varepsilon_2\}^T \cdot \{R\} + \{\delta\varepsilon^I\}^T \cdot \{N^I\} + \{\delta\varepsilon_{NL}\}^T \cdot \{N_T^0\}] d\Omega = 0, \tag{6}$$

where $\{N\}^T = \{N_{xx} \;\; N_{yy} \;\; N_{xy} \;\; Q_{xz} \;\; Q_{yz} \;\; Q_{zz}\}$, $\{M\}^T = \{0 \;\; 0 \;\; 0 \;\; M_{xz} \;\; M_{yz} \;\; M_{zz}\}$, $\{R\}^T = \{0 \;\; 0 \;\; 0 \;\; R_{xz} \;\; R_{yz} \;\; 0\}$ and $\{N^I\} = \left\{N_{xx}^I \;\; N_{yy}^I \;\; N_{xy}^I \;\; Q_{xz}^I \;\; Q_{yz}^I \;\; 0\right\}$ are the stress resultants in middle and Ith plane, while $\{N_T^0\}^T = \left\{N_{Txx}^0 \;\; N_{Tyy}^0 \;\; N_{Txy}^0 \;\; 0 \;\; 0 \;\; 0\right\}$ are in-plane thermal force given as:

$$\begin{Bmatrix} N\\ N^I\end{Bmatrix} = \begin{bmatrix} [A] & [E] & [F] & \sum_{I=1}^{N}[B^I]\\ [B^I] & [H^I] & [L^I] & \sum_{J=1}^{N}[D^{IJ}]\end{bmatrix} \cdot \begin{Bmatrix}\{\varepsilon_{0L}\}\\ \{\varepsilon_1\}\\ \{\varepsilon_2\}\\ \{\varepsilon_I\}\end{Bmatrix},$$

$$\begin{Bmatrix} M\\ R\end{Bmatrix} = \begin{bmatrix} [E] & [F] & [G] & \sum_{I=1}^{N}[H^I]\\ [F] & [G] & [R] & \sum_{I=1}^{N}[L^I]\end{bmatrix} \cdot \begin{Bmatrix}\{\varepsilon_{0L}\}\\ \{\varepsilon_1\}\\ \{\varepsilon_2\}\\ \{\varepsilon_I\}\end{Bmatrix},$$

$$\{N_T^0\} = -\sum_{k=1}^{N}\int_{z_k}^{z_{k+1}} [Q]^{(k)}\{\alpha\}^{(k)} \cdot \Delta T \, dz, \tag{7}$$

where the material stiffness coefficient are given as:

$$([A_{ij}], [E_{ij}], [F_{ij}], [G_{ij}], [R_{ij}]) = \sum_{k=1}^{n}\int_{z_k}^{z_{k+1}} [Q_{ij}]^{(k)}(1, \;\; z, \;\; z^2, \;\; z^3, \;\; z^4)\, dz,$$

$$\left(\left[B_{ij}^I\right], \left[H_{ij}^I\right], \left[L_{ij}^I\right]\right) = \sum_{k=1}^{n}\int_{z_k}^{z_{k+1}} [Q_{ij}]^{(k)}\left[\Phi^I\right] \cdot (1, \;\; z, \;\; z^2)\, dz,$$

$$\left[D_{ij}^{IJ}\right] = \sum_{k=1}^{n}\int_{z_k}^{z_{k+1}} [Q_{ij}]^{(k)} \cdot [\Phi^I] \cdot \left[\Phi^J\right] dz. \tag{8}$$

Integrating the displacement gradients by parts in Eq. (6) with respect to x and y, and collecting the coefficients of $\delta u_0, \delta v_0, \delta w_0, \delta w_1, \delta w_2, \delta U^I, \delta V^I$, the following Euler–Lagrange governing equations of the Present LW Theory defining thermal buckling of laminated composite plates are obtained:

$$\begin{aligned}
\delta u_0: &\quad -N_{xx,x} - N_{xy,y} = 0,\\
\delta v_0: &\quad -N_{xy,x} - N_{yy,y} = 0,\\
\delta w_0: &\quad -Q_{xz,x} - Q_{yz,y} + \eta_0(w) = 0,\\
\delta w_1: &\quad -M_{xz,x} - M_{yz,x} + Q_{zz} + \eta_1(w) = 0,\\
\delta w_2: &\quad -R_{xz,x} - R_{yz,x} + 2M_{zz} + \eta_2(w) = 0,\\
\delta U^I: &\quad -N_{xx,x}^I - N_{xy,y}^I + Q_{xz}^I = 0,\\
\delta V^I: &\quad -N_{xy,x}^I - N_{yy,y}^I + Q_{yz}^I = 0,
\end{aligned} \tag{9}$$

where $\eta_0(w) = \frac{\partial}{\partial x}\left(N_{Txx}^0\frac{\partial w}{\partial x} + N_{Txy}^0\frac{\partial w}{\partial y}\right) + \frac{\partial}{\partial y}\left(N_{Tyy}^0\frac{\partial w}{\partial y} + N_{Txy}^0\frac{\partial w}{\partial x}\right)$, $\eta_1(w) = \frac{\partial}{\partial x}\left(M_{Txx}^0\frac{\partial w}{\partial x} + M_{Txy}^0\frac{\partial w}{\partial y}\right) + \frac{\partial}{\partial y}\left(M_{Tyy}^0\frac{\partial w}{\partial y} + M_{Txy}^0\frac{\partial w}{\partial x}\right)$, $\eta_2(w) = \frac{\partial}{\partial x}\left(R_{Txx}^0\frac{\partial w}{\partial x} + R_{Txy}^0\frac{\partial w}{\partial y}\right) + \frac{\partial}{\partial y}\left(R_{Tyy}^0\frac{\partial w}{\partial y} + R_{Txy}^0\frac{\partial w}{\partial x}\right)$, with appropriate mechanical boundary conditions:

$$\begin{aligned}
\delta u_0: &\quad N_{xx}n_x + N_{xy}n_y = \overline{N}_{xx}n_x + \overline{N}_{xy}n_y,\\
\delta v_0: &\quad N_{xy}n_x + N_{yy}n_y = \overline{N}_{xy}n_x + \overline{N}_{yy}n_y,\\
\delta w_0: &\quad Q_{xz}n_x + Q_{yz}n_y = \overline{Q}_{xz}n_x + \overline{Q}_{yz}n_y,\\
\delta w_1: &\quad M_{xz}n_x + M_{yz}n_y = \overline{M}_{xz}n_x + \overline{M}_{yz}n_y,\\
\delta w_2: &\quad R_{xz}n_x + R_{yz}n_y = \overline{R}_{xz}n_x + \overline{R}_{yz}n_y,\\
\delta U^I: &\quad N_{xx}^I n_x + N_{xy}^I n_y = \overline{N}_{xx}^I n_x + \overline{N}_{xy}^I n_y,\\
\delta V^I: &\quad N_{xy}^I n_x + N_{yy}^I n_y = \overline{N}_{xy}^I n_x + \overline{N}_{yy}^I n_y.
\end{aligned} \tag{10}$$

In order to discretize the governing equations, the explicit form of Euler–Lagrange governing equations in terms of displacements are given as:

$$\begin{aligned}
\delta u_0: &\quad -A_{11}u_{0,xx} - A_{12}v_{0,yx} - A_{16}w_{1,x} - 2E_{16}w_{2,x} - A_{33}(u_{0,yy} + v_{0,xy})\\
&\quad -\sum_{I=1}^{N}\left[B_{11}^I U_{,xx}^I + B_{12}^I V_{,xx}^I + B_{33}^I\left(U_{,xx}^I + V_{,xy}^I\right)\right] = 0,\\
\delta v_0: &\quad -A_{33}(u_{0,yx} + v_{0,xx}) - A_{12}u_{0,yx} - A_{22}v_{0,yy} - A_{26}w_{1,y} - 2E_{26}w_{2,y}\\
&\quad -\sum_{I=1}^{N}\left[B_{12}^I U_{,xy}^I + B_{22}^I V_{,yy}^I + B_{33}^I\left(U_{,xy}^I + V_{,xx}^I\right)\right] = 0,
\end{aligned}$$

$$
\begin{aligned}
\delta w_0:\ & -A_{44}w_{0,xx}-E_{44}w_{1,xx}-F_{44}w_{2,xx}-A_{55}w_{0,yy}-E_{55}w_{1,yy}\\
& -F_{55}w_{2,yy}-\sum_{I=1}^{N}\left[B_{44}^{I}U_{,x}^{I}+B_{55}^{I}V_{,y}^{I}\right]\\
& +\left(N_{Txx}^{0}w_{0,xx}+2N_{Txy}^{0}w_{0,xy}+N_{Tyy}^{0}w_{0,yy}\right)\\
& +\left(M_{Txx}^{0}w_{1,xx}+2M_{Txy}^{0}w_{1,xy}+M_{Tyy}^{0}w_{1,yy}\right)\\
& +\left(R_{Txx}^{0}w_{2,xx}+2R_{Txy}^{0}w_{2,xy}+R_{Tyy}^{0}w_{2,yy}\right)=0,\\
\delta w_1:\ & -E_{44}w_{0,xx}-F_{44}w_{1,xx}-G_{44}w_{2,xx}-E_{55}w_{0,yy}-F_{55}w_{1,yy}\\
& -G_{55}w_{2,yy}+A_{66}w_1+2E_{66}w_2+A_{16}u_{0,x}+A_{26}v_{0,y}\\
& +\sum_{I=1}^{N}\left[B_{16}^{I}U_{,x}^{I}+B_{26}^{I}V_{,y}^{I}\right]-\sum_{I=1}^{N}\left[H_{44}^{I}U_{,x}^{I}+H_{55}^{I}V_{,y}^{I}\right]\\
& +\left(M_{Txx}^{0}w_{0,xx}+2M_{Txy}^{0}w_{0,xy}+M_{Tyy}^{0}w_{0,yy}\right)\\
& +\left(R_{Txx}^{0}w_{1,xx}+2R_{Txy}^{0}w_{1,xy}+R_{Tyy}^{0}w_{1,yy}\right)\\
& +\left(S_{Txx}^{0}w_{2,xx}+2S_{Txy}^{0}w_{2,xy}+S_{Tyy}^{0}w_{2,yy}\right)=0,\\
\delta w_2:\ & -F_{44}w_{0,xx}-G_{44}w_{1,xx}-R_{44}w_{2,xx}-F_{55}w_{0,yy}-G_{55}w_{1,yy}\\
& -R_{55}w_{2,yy}+2E_{66}w_1+4F_{66}w_2+2E_{16}u_{0,x}+2E_{26}v_{0,y}\\
& +\sum_{I=1}^{N}2\left[H_{16}^{I}U_{,x}^{I}+H_{26}^{I}V_{,y}^{I}\right]-\sum_{I=1}^{N}\left[L_{44}^{I}U_{,x}^{I}+L_{55}^{I}V_{,y}^{I}\right]\\
& +\left(R_{Txx}^{0}w_{0,xx}+2R_{Txy}^{0}w_{0,xy}+R_{Tyy}^{0}w_{0,yy}\right)\\
& +\left(S_{Txx}^{0}w_{1,xx}+2S_{Txy}^{0}w_{1,xy}+S_{Tyy}^{0}w_{1,yy}\right)\\
& +\left(P_{Txx}^{0}w_{2,xx}+2P_{Txy}^{0}w_{2,xy}+P_{Tyy}^{0}w_{2,yy}\right)=0,\\
\delta U^I:\ & -B_{11}^{I}u_{0,xx}-B_{12}^{I}v_{0,yx}-B_{16}^{I}w_{1,x}-2H_{16}^{I}w_{2,x}-B_{33}^{I}\left(u_{0,yy}+v_{0,xy}\right)\\
& +B_{44}^{I}w_{0,x}+H_{44}^{I}w_{1,x}+L_{44}^{I}w_{2,x}\\
& -\sum_{J=1}^{N}\left[D_{11}^{IJ}U_{,xx}^{J}+D_{12}^{IJ}V_{,yx}^{J}+D_{33}^{IJ}\left(U_{,yy}^{J}+V_{,xy}^{J}\right)-D_{44}^{IJ}U^{J}\right]=0,\\
\delta V^I:\ & -B_{33}^{I}\left(u_{0,yx}+v_{0,xx}\right)-B_{12}^{I}u_{0,xy}-B_{22}^{I}v_{0,yy}-B_{26}^{I}w_{1,y}\\
& -2H_{26}^{I}w_{2,y}+B_{55}^{I}w_{0,y}+H_{55}^{I}w_{1,y}+L_{55}^{I}w_{2,y}\\
& -\sum_{J=1}^{N}\left[D_{33}^{IJ}\left(U_{,yx}^{J}+V_{,xx}^{J}\right)+D_{12}^{IJ}U_{,xy}^{J}+D_{22}^{IJ}V_{,yy}^{J}-D_{55}^{IJ}V^{J}\right]=0.
\end{aligned}
$$

$$
\begin{aligned}
&\text{where}:\ \left(\{\boldsymbol{N_T^0}\},\ \{\boldsymbol{M_T^0}\},\ \{\boldsymbol{R_T^0}\},\ \{\boldsymbol{S_T^0}\},\ \{\boldsymbol{P_T^0}\}\right)\\
&=\int_{-h/2}^{h/2}\left(1,\ z,\ z^2,\ z^3,\ z^4\right)\left\{\sigma_{Txx}^{0}\ \ \sigma_{Tyy}^{0}\ \ \sigma_{Txy}^{0}\right\}dz
\end{aligned}
\tag{11}
$$

2.3. Governing equations of the Layerwise Theory of Reddy

2.3.1. Displacement field

The displacements components (u, v, w) at a point (x, y, z) are expressed as:

$$
\begin{aligned}
u(x,y,z)&=u_0(x,y)+\sum_{I=1}^{N}U^I(x,y)\cdot\Phi^I(z),\\
v(x,y,z)&=v_0(x,y)+\sum_{I=1}^{N}V^I(x,y)\cdot\Phi^I(z),\\
w(x,y,z)&=w_0(x,y),
\end{aligned}
\tag{12}
$$

where (u_0, v_0, w_0) are displacements of a point $(x, y, 0)$ on the reference plane of the laminate, functions $\Phi^I(z)$ are one-dimensional linear Lagrange interpolation functions of thickness coordinates and (U^I, V^I) are the values of (u, v) at the Ith plane.

2.3.2. Strain displacement relations

The strains associated with the displacement field (12) are computed using von Karman's non-linear strain–displacement relation:

$$
\begin{Bmatrix}\varepsilon_{xx}\\ \varepsilon_{yy}\\ \gamma_{xy}\\ \gamma_{xz}\\ \gamma_{yz}\end{Bmatrix}=\begin{Bmatrix}\frac{\partial u}{\partial x}+\frac{1}{2}\left(\frac{\partial w_0}{\partial x}\right)^2\\ \frac{\partial v}{\partial y}+\frac{1}{2}\left(\frac{\partial w_0}{\partial x}\right)^2\\ \frac{\partial u}{\partial y}+\frac{\partial v}{\partial y}+\frac{\partial w_0}{\partial x}\frac{\partial w_0}{\partial y}\\ \frac{\partial u}{\partial z}+\frac{\partial w_0}{\partial x}\\ \frac{\partial v}{\partial z}+\frac{\partial w_0}{\partial y}\end{Bmatrix}=\{\varepsilon_{0L}\}+\{\varepsilon_{0NL}\}+\sum_{I=1}^{N}\left[\Phi^I\right]\cdot\{\varepsilon_I\},
\tag{13}
$$

where:

$$
\{\varepsilon_{0L}\}^T=\left\{\frac{\partial u_0}{\partial x}\ \ \frac{\partial v_0}{\partial y}\ \ \frac{\partial u_0}{\partial y}+\frac{\partial v_0}{\partial x}\ \ \frac{\partial w_0}{\partial x}\ \ \frac{\partial w_0}{\partial y}\right\},
$$

$$
\{\varepsilon_{0NL}\}^T=\left\{\frac{1}{2}\left(\frac{\partial w_0}{\partial x}\right)^2\ \ \frac{1}{2}\left(\frac{\partial w_0}{\partial y}\right)^2\ \ \frac{\partial w_0}{\partial x}\frac{\partial w_0}{\partial y}\ \ 0\ \ 0\right\},
$$

$$
\{\varepsilon_I\}^T=\left\{\frac{\partial U^I}{\partial x}\ \ \frac{\partial V^I}{\partial x}\ \ \frac{\partial U^I}{\partial y}+\frac{\partial V^I}{\partial x}\ \ U^I\ \ V^I\right\},
$$

$$
\left[\Phi^I\right]=\begin{bmatrix}\Phi^I & & & & \\ & \Phi^I & & & \\ & & \Phi^I & & \\ & & & \frac{d\Phi^I}{dz} & \\ & & & & \frac{d\Phi^I}{dz}\end{bmatrix}.
$$

2.3.3. Constitutive equations

The stress–strain relations for kth orthotropic lamina in global coordinates are given as:

$$
\begin{Bmatrix}\sigma_{xx}\\ \sigma_{yy}\\ \tau_{xy}\\ \tau_{xz}\\ \tau_{yz}\end{Bmatrix}^{(k)}=\begin{bmatrix}Q_{11} & Q_{12} & Q_{13} & 0 & 0\\ & Q_{22} & Q_{23} & 0 & 0\\ & & Q_{33} & 0 & 0\\ \textit{symmetric} & & & Q_{44} & Q_{45}\\ & & & & Q_{55}\end{bmatrix}^{(k)}\times\left(\begin{Bmatrix}\varepsilon_{xx}\\ \varepsilon_{yy}\\ \gamma_{xy}\\ \gamma_{xz}\\ \gamma_{yz}\end{Bmatrix}^{(k)}-\begin{Bmatrix}\alpha_{xx}\\ \alpha_{yy}\\ \alpha_{xy}\\ 0\\ 0\end{Bmatrix}^{(k)}\cdot\Delta T\right),
\tag{14}
$$

where $\boldsymbol{\sigma}^{(k)}=\{\sigma_{xx}\ \ \sigma_{yy}\ \ \tau_{xy}\ \ \tau_{xz}\ \ \tau_{yz}\}^{(k)^T}$ and $\boldsymbol{\varepsilon}^{(k)}=\{\varepsilon_{xx}\ \ \varepsilon_{yy}\ \ \gamma_{xy}\ \ \gamma_{xz}\ \ \gamma_{yz}\}^{(k)^T}$ are stress and strain components, respectively, and $\mathbf{Q}_{ij}^{(k)}$ are transformed elastic coefficients, of kth lamina in global coordinates, $\alpha^{(k)}=\{\alpha_{xx}\ \ \alpha_{yy}\ \ \alpha_{xy}\ \ 0\ \ 0\}^{(k)^T}$ are coefficients of thermal expansion, of kth lamina in global coordinates, while ΔT is temperature rise.

2.3.4. Governing equations and boundary conditions

The governing equations of the Present LW Theory are derived using the principle of virtual displacements (PVD). After performing the integration in the thickness direction the internal work and external work due to in-plane thermal forces become:

$$
\delta V+\delta U=\int_{\Omega}\left[\{\delta\varepsilon_{0L}\}^T\cdot\{N\}+\{\delta\varepsilon^I\}^T\cdot\{N^I\}+\{\delta\varepsilon_{0NL}\}^T\cdot\{N_T^0\}\right]d\Omega=0,
\tag{15}
$$

where $\{N\}=\{N_{xx}\ \ N_{yy}\ \ N_{xy}\ \ Q_{xz}\ \ Q_{yz}\}^T$, $\{N^I\}=\{N_{xx}^I\ \ N_{yy}^I\ \ N_{xy}^I\ \ Q_{xz}^I\ \ Q_{yz}^I\}^T$ and $\{N_T^0\}=\{N_{Txx}^0\ \ N_{Tyy}^0\ \ N_{Txy}^0\ \ 0\ \ 0\}^T$ are the stress resultants in middle and Ith plane, given as:

$$\begin{Bmatrix} N \\ N^I \end{Bmatrix} = \begin{bmatrix} [A] & \sum_{I=1}^{N}[B^I] \\ [B^I] & \sum_{J=1}^{N}[D^{JI}] \end{bmatrix} \cdot \begin{Bmatrix} \{\varepsilon_{0L}\} \\ \{\varepsilon^I\} \end{Bmatrix} dz,$$

$$\{N_T^0\} = -\sum_{k=1}^{N}\int_{z_k}^{z_{k+1}} [\mathbf{Q}]^{(k)}\{\alpha\}^{(k)} \cdot \Delta T\, dz, \tag{16}$$

where the material stiffness coefficient $[\boldsymbol{A}]$, $[\boldsymbol{B^I}]$, $[\boldsymbol{D^{IJ}}]$ are given in [52].

Integrating the displacement gradients by parts in Eq. (15) with respect to x and y, and collecting the coefficients of $\delta u_0, \delta v_0, \delta w_0, \delta U^I, \delta V^I$, the following Euler–Lagrange governing equations of the Reddy's LW theory defining thermal buckling of laminated composite plates are obtained:

$$\begin{aligned}
\delta u_0 &: \quad -N_{xx,x} - N_{xy,y} = 0,\\
\delta v_0 &: \quad -N_{xy,x} - N_{yy,y} = 0,\\
\delta w_0 &: \quad -Q_{xz,x} - Q_{yz,y} + \eta(w) = 0,\\
\delta U^I &: \quad -N^I_{xx,x} - N^I_{xy,y} + Q^I_{xz} = 0,\\
\delta V^I &: \quad -N^I_{xy,x} - N^I_{yy,y} + Q^I_{yz} = 0,
\end{aligned} \tag{17}$$

where $\eta(w) = \frac{\partial}{\partial x}\left(N^0_{Txx}\frac{\partial w}{\partial x} + N^0_{Txy}\frac{\partial w}{\partial y}\right) + \frac{\partial}{\partial y}\left(N^0_{Tyy}\frac{\partial w}{\partial y} + N^0_{Txy}\frac{\partial w}{\partial x}\right)$, with appropriate mechanical boundary conditions:

$$\begin{aligned}
\delta u_0 &: \quad N_{xx}n_x + N_{xy}n_y = \overline{N}_{xx}n_x + \overline{N}_{xy}n_y,\\
\delta v_0 &: \quad N_{xy}n_x + N_{yy}n_y = \overline{N}_{xy}n_x + \overline{N}_{yy}n_y,\\
\delta w_0 &: \quad Q_{xz}n_x + Q_{yz}n_y = \overline{Q}_{xz}n_x + \overline{Q}_{yz}n_y,\\
\delta U^I &: \quad N^I_{xx}n_x + N^I_{xy}n_y = \overline{N}^I_{xx}n_x + \overline{N}^I_{xy}n_y,\\
\delta V^I &: \quad N^I_{xy}n_x + N^I_{yy}n_y = \overline{N}^I_{xy}n_x + \overline{N}^I_{yy}n_y.
\end{aligned} \tag{18}$$

In order to discretize the governing equations, the explicit form of Euler–Lagrange governing equations in terms of displacements are given in [52].

3. Finite element model

3.1. Finite element of the Present LW Theory

3.1.1. Displacement field

The finite element of the Present LW Theory consists of middle surface plane and $I = 1, N$ planes through the thickness of the plate, Fig. 2. In each node the following generalized displacement components are adopted, that are $(u_0, v_0, w_0, w_1, w_2)$ in the middle surface element nodes and (U^I, V^I) in the Ith plane element nodes. The generalized displacements over finite element Ω^e are expressed as:

$$\begin{Bmatrix} u \\ v \\ w \\ w_1 \\ w_2 \end{Bmatrix}^e = \begin{Bmatrix} \sum_{j=1}^{m} u_{0j}\Psi_j \\ \sum_{j=1}^{m} v_{0j}\Psi_j \\ \sum_{j=1}^{m} w_{0j}\Psi_j \\ \sum_{j=1}^{m} w_{1j}\Psi_j \\ \sum_{j=1}^{m} w_{2j}\Psi_j \end{Bmatrix}^e = \sum_{j=1}^{m}[\boldsymbol{\Psi}_j]^e\{\boldsymbol{d}_j\}^e,$$

$$\begin{Bmatrix} U^I \\ V^I \end{Bmatrix}^e = \begin{Bmatrix} \sum_{j=1}^{m} U^I_j\Psi_j \\ \sum_{j=1}^{m} V^I_j\Psi_j \end{Bmatrix}^e = \sum_{j=1}^{m}[\bar{\boldsymbol{\Psi}}_j]^e\{\boldsymbol{d}^I_j\}^e, \tag{19}$$

where $\{\boldsymbol{d}_j\}^e = \{\, u^e_{0j} \quad v^e_{0j} \quad w^e_{0j} \quad w^e_{1j} \quad w^e_{2j} \,\}^T$, $\left\{\boldsymbol{d}^I_j\right\}^e = \left\{\, U^I_j \quad V^I_j \,\right\}^T$ are generalized displacement vectors in the middle plane and Ith plane, respectively, while Ψ^e_j and $[\bar{\Psi}_j]^e$ are interpolation functions given as:

$$[\boldsymbol{\psi_j}]^e = \begin{bmatrix} \psi_m & & & & \\ & \psi_m & & & \\ & & \psi_m & & \\ & & & \psi_m & \\ & & & & \psi_m \end{bmatrix}, \quad [\bar{\boldsymbol{\psi}}_{\boldsymbol{j}}]^e = \begin{bmatrix} \psi_m & \\ & \psi_m \end{bmatrix}. \tag{20}$$

3.1.2. Geometry of the element

The geometry of the element is interpolated with the same interpolation functions over the element Ω^e, as the generalized displacements, thus isoparametric finite element formulation is adopted.

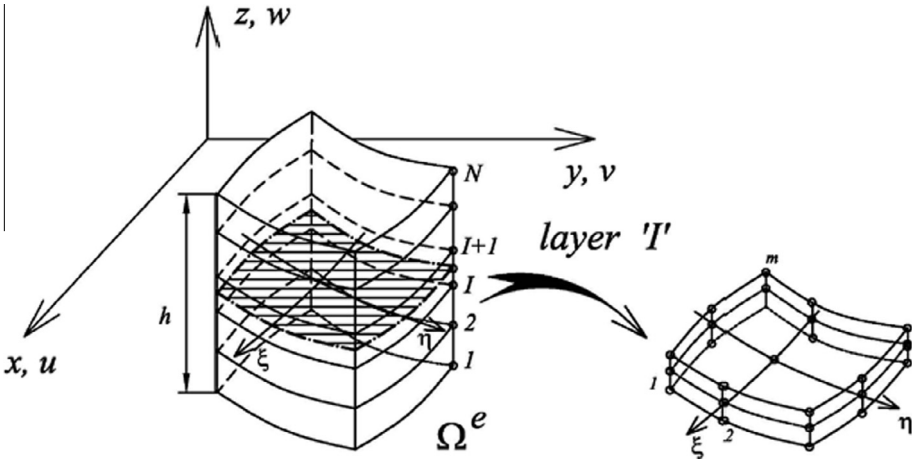

Fig. 2. Plate finite element with n layers and m nodes.

$$\begin{Bmatrix} x \\ y \\ z \end{Bmatrix}^e = \begin{Bmatrix} \sum_{j=1}^{m} x_j \Psi_j \\ \sum_{j=1}^{m} y_j \Psi_j \\ \sum_{j=1}^{m} z_j \Psi_j \end{Bmatrix}^e, \tag{21}$$

where $\{x_j \quad y_j \quad z_j\}$ are $\{x \quad y \quad z\}$ coordinates of jth node of the element Ω^e.

3.1.3. Strain field

The strain–displacement relations (2) over the finite element Ω^e is expressed as:

$$\{\varepsilon_{0L}\} = \sum_{j=1}^{m} [\boldsymbol{H_j}] \{\boldsymbol{d_j}\}^e, \quad \{\varepsilon_1\} = \sum_{j=1}^{m} [\boldsymbol{H_{1j}}] \{\boldsymbol{d_j}\}^e, \quad \{\varepsilon_2\} = \sum_{j=1}^{m} [\boldsymbol{H_{2j}}] \{\boldsymbol{d_j}\}^e,$$
$$\{\varepsilon^l\} = \sum_{j=1}^{m} [\overline{\boldsymbol{H}}_{\boldsymbol{j}}] \left\{\boldsymbol{d}_j^l\right\}^e, \tag{22}$$

where:

$$[\boldsymbol{H_j}] = \begin{bmatrix} \frac{\partial \psi_j}{\partial x} & 0 & 0 & 0 & 0 \\ 0 & \frac{\partial \psi_j}{\partial y} & 0 & 0 & 0 \\ \frac{\partial \psi_j}{\partial y} & \frac{\partial \psi_j}{\partial x} & 0 & 0 & 0 \\ 0 & 0 & \frac{\partial \psi_j}{\partial x} & 0 & 0 \\ 0 & 0 & \frac{\partial \psi_j}{\partial y} & 0 & 0 \\ 0 & 0 & 0 & 1 & 0 \end{bmatrix}, \quad [\boldsymbol{H_{1j}}] = \begin{bmatrix} 0 & 0 & 0 & 0 & 0 \\ 0 & 0 & 0 & 0 & 0 \\ 0 & 0 & 0 & 0 & 0 \\ 0 & 0 & 0 & \frac{\partial \psi_j}{\partial x} & 0 \\ 0 & 0 & 0 & \frac{\partial \psi_j}{\partial y} & 0 \\ 0 & 0 & 0 & 0 & 2 \end{bmatrix},$$
$$[\boldsymbol{H_{2j}}] = \begin{bmatrix} 0 & 0 & 0 & 0 & 0 \\ 0 & 0 & 0 & 0 & 0 \\ 0 & 0 & 0 & 0 & 0 \\ 0 & 0 & 0 & 0 & \frac{\partial \psi_j}{\partial x} \\ 0 & 0 & 0 & 0 & \frac{\partial \psi_j}{\partial y} \\ 0 & 0 & 0 & 0 & 0 \end{bmatrix}, \quad [\overline{\boldsymbol{H}}_{\boldsymbol{j}}] = \begin{bmatrix} \frac{\partial \psi_j}{\partial x} & 0 \\ 0 & \frac{\partial \psi_j}{\partial y} \\ \frac{\partial \psi_j}{\partial y} & \frac{\partial \psi_j}{\partial x} \\ \psi_j & 0 \\ 0 & \psi_j \\ 0 & 0 \end{bmatrix}. \tag{23}$$

3.1.4. Governing equations

Substituting previously defined strain field (22) into the virtual work statement (6), the buckling equations over the finite element Ω^e are obtained as:

$$\left([\boldsymbol{K}]^e - \Delta T_{cr} [\boldsymbol{K}_G]^e\right) \{\Delta\}^e = \{\boldsymbol{0}\}, \tag{24}$$

where stiffness matrix $[\boldsymbol{K}]^e$ for the finite element Ω^e is given as:

$$[\boldsymbol{K}]^{\boldsymbol{e}} = \int_{\Omega^e} \begin{bmatrix} [\boldsymbol{K^{11}}]^{\boldsymbol{e}} & [\boldsymbol{K^{12}}]^{\boldsymbol{e}} \\ [\boldsymbol{K^{21}}]^{\boldsymbol{e}} & [\boldsymbol{K^{22}}]^{\boldsymbol{e}} \end{bmatrix} d\Omega^e, \tag{25}$$

where:

$$[\boldsymbol{K^{11}}]^{\boldsymbol{e}} = \sum_{i=1}^{m}\sum_{j=1}^{n} [H_i]^T [A] [H_j] + [H_i]^T [E] [H_{1j}] + [H_i]^T [F] [H_{2j}] + [H_{1i}]^T [E] [H_j] + [H_{1j}]^T [F] [H_{1j}] + [H_{1j}]^T [G] [H_{2j}] + [H_{2j}]^T [F] [H_j] + [H_{2j}]^T [G] [H_{1j}] + [H_{2j}]^T [R] [H_{2j}],$$

$$[\boldsymbol{K^{12}}]^{\boldsymbol{e}} = \sum_{i=1}^{m}\sum_{j=1}^{n} [H_i]^T [B^l] [\overline{H}_j] + [H_{1i}]^T [H^l] [\overline{H}_j] + [H_{2i}]^T [L^l] [\overline{H}_j],$$

$$[\boldsymbol{K^{21}}]^{\boldsymbol{e}} = \sum_{i=1}^{m}\sum_{j=1}^{n} [\overline{H}_i]^T [B^l] [H_j] + [\overline{H}_i]^T [H^l] [H_{1j}] + [\overline{H}_i]^T [L^l] [H_{2j}],$$

$$[\boldsymbol{K^{22}}]^{\boldsymbol{e}} = \sum_{i=1}^{m}\sum_{j=1}^{n} [\overline{H}_i]^T [D^{ll}] [\overline{H}_j], \tag{26}$$

while element geometric stiffness matrix for the element Ω^e is:

$$\boldsymbol{K}_G^e = \int_{\Omega^e}\int_{-h/2}^{h/2} \begin{bmatrix} [\boldsymbol{G}_i^e]^{\boldsymbol{T}} [\boldsymbol{\sigma}_T^0] [\boldsymbol{G}_j^e] & 0 \\ 0 & 0 \end{bmatrix} dz\, d\Omega^e, \tag{27}$$

$$\text{where:} \quad [\boldsymbol{G}_i]^e = \begin{bmatrix} 0 & 0 & \frac{\partial \Psi_i^e}{\partial x} & z\frac{\partial \Psi_i^e}{\partial x} & z^2\frac{\partial \Psi_i^e}{\partial x} \\ 0 & 0 & \frac{\partial \Psi_i^e}{\partial y} & z\frac{\partial \Psi_i^e}{\partial y} & z^2\frac{\partial \Psi_i^e}{\partial y} \end{bmatrix}, \quad [\boldsymbol{\sigma}_T^0] = \begin{bmatrix} \sigma_{Txx}^0 & \sigma_{Txy}^0 \\ \sigma_{Txy}^0 & \sigma_{Tyy}^0 \end{bmatrix},$$
$$\{\Delta\}^e = \begin{Bmatrix} \{\boldsymbol{d}\} \\ \left\{\sum_{l=1}^{N} \boldsymbol{d}^l\right\} \end{Bmatrix}^e. \tag{28}$$

Solution of equations (24) gives eigenvalues $\Delta T_1, \Delta T_2, \ldots \Delta T_N$. The smallest of the eigenvalues not equal to zero is the critical temperature ΔT_{cr} and the corresponding eigenvector is buckling mode.

3.2. Finite element of the Reddy's LW Theory

3.2.1. Displacement field

The finite element of Reddy's LW theory requires only the C^0 continuity of major unknowns, thus in each node only a displacement components are adopted, that are (u_0, v_0, w_0) in the middle surface element nodes and (U^l, V^l) in the lth plane element nodes. The generalized displacements over finite element Ω^e are expressed as:

$$\begin{Bmatrix} u \\ v \\ w \end{Bmatrix}^e = \begin{Bmatrix} \sum_{j=1}^{m} u_{0j} \Psi_j \\ \sum_{j=1}^{m} v_{0j} \Psi_j \\ \sum_{j=1}^{m} w_{0j} \Psi_j \end{Bmatrix}^e = \sum_{j=1}^{m} [\boldsymbol{\Psi_j}]^e \{\boldsymbol{d}_j\}^e,$$
$$\begin{Bmatrix} U^l \\ V^l \end{Bmatrix}^e = \begin{Bmatrix} \sum_{j=1}^{m} U_j^l \Psi_j \\ \sum_{j=1}^{m} V_j^l \Psi_j \end{Bmatrix}^e = \sum_{j=1}^{m} [\bar{\boldsymbol{\Psi}}_{\boldsymbol{j}}]^e \{\boldsymbol{d}_j^l\}^e, \tag{29}$$

where $\{\boldsymbol{d}_j\}^e = \{u_{0j}^e \quad v_{0j}^e \quad w_{0j}^e\}^T$, $\{\boldsymbol{d}_j^l\}^e = \left\{U_j^l \quad V_j^l\right\}^T$ are displacement vectors in the middle plane and lth plane, respectively, and Ψ_j^e are interpolation functions, for the jth node of the element Ω^e, while $[\boldsymbol{\Psi_j}]^e$ and $[\bar{\boldsymbol{\Psi}}_{\boldsymbol{j}}]^e$ are given in [51].

3.2.2. Geometry of the element

The geometry of the element is interpolated with the same interpolation functions over the element Ω^e, as the generalized displacements, thus isoparametric finite element formulation is adopted, as given in (21).

3.2.3. Strain field

The strain–displacement relations (13) over the finite element Ω^e are expressed as:

$$\{\varepsilon_{0L}\} = \sum_{j=1}^{m} [\boldsymbol{H_j}] \{\boldsymbol{d_j}\}^e, \quad \{\varepsilon^l\} = \sum_{j=1}^{m} [\overline{\boldsymbol{H}}_{\boldsymbol{j}}] \{\boldsymbol{d}_j^l\}^e, \tag{30}$$

where $[\boldsymbol{H_j}]$ and $[\overline{\boldsymbol{H}}_{\boldsymbol{j}}]$ are given in [51].

3.2.4. Governing equations

Substituting previously defined strain field (30) into the virtual work statement (15), buckling equations over the finite element Ω^e are obtained as:

$$\left([\boldsymbol{K}]^e - \Delta T_{cr}[\boldsymbol{K}_G]^e\right)\{\boldsymbol{\Delta}\}^e = \{\boldsymbol{0}\}, \tag{31}$$

where stiffness matrix $[\boldsymbol{K}]^e$ for the finite element Ω^e is given in [51], while element geometric stiffness matrix for the element Ω^e is:

$$\boldsymbol{K}_G^e = \int_{\Omega^e} \begin{bmatrix} [\boldsymbol{G}_i^e]^T [\boldsymbol{N}_T^0] [\boldsymbol{G}_j^e] & 0 \\ 0 & 0 \end{bmatrix} d\Omega^e, \tag{32}$$

$$\text{where}: \quad [\boldsymbol{G}_i]^e = \begin{bmatrix} 0 & 0 & \frac{\partial \Psi_i^e}{\partial x} \\ 0 & 0 & \frac{\partial \Psi_i^e}{\partial y} \end{bmatrix}, \quad [\boldsymbol{N}_T^0] = \begin{bmatrix} N_{Txx}^0 & N_{Txy}^0 \\ N_{Txy}^0 & N_{Tyy}^0 \end{bmatrix},$$

$$\{\boldsymbol{\Delta}\}^e = \begin{Bmatrix} \{\boldsymbol{d}\} \\ \left\{\sum_{I=1}^{N} \boldsymbol{d}^I\right\} \end{Bmatrix}^e. \tag{33}$$

Solution of equations (31) gives eigenvalues $\Delta T_1, \Delta T_2, \ldots \Delta T_N$. The smallest of the eigenvalues not equal to zero is the critical temperature ΔT_{cr} and the corresponding eigenvector is buckling mode.

4. Analytical solutions

4.1. Analytical solution of the Present LW Theory

In order to verify the accuracy of finite element solution, wherever appropriate 3D elasticity solution is not available, analytical solutions may be used. Navier's solution of the Present LW Theory is derived for the rectangular cross-ply laminated plates *axb* with the following simply supported boundary conditions:

$$v_0 = w_0 = w_2 = V^I = N_{xx} = N_{xx}^I = 0 \quad \text{at} \quad x = 0,\ a,$$

$$u_0 = w_0 = w_2 = U^I = N_{yy} = N_{yy}^I = 0 \quad \text{at} \quad y = 0,\ b. \tag{34}$$

The displacement field which satisfies the boundary conditions (34) and Euler–Lagrange equilibrium equations (11), is given in the form:

$$\left[u_0(x,y); U^I(x,y)\right] = \sum_{m=1}^{\infty}\sum_{n=1}^{\infty}\left[u_{0mn}; U_{mn}^I\right] \cdot \cos\frac{m\pi}{a}x \cdot \sin\frac{n\pi}{b}y,$$

$$\left[v_0(x,y); V^I(x,y)\right] = \sum_{m=1}^{\infty}\sum_{n=1}^{\infty}\left[v_{0mn}; V_{mn}^I\right] \cdot \sin\frac{m\pi}{a}x \cdot \cos\frac{n\pi}{b}y,$$

$$[w_0(x,y), w_1(x,y), w_2(x,y)] = \sum_{m=1}^{\infty}\sum_{n=1}^{\infty}\left[W_{mn}^0, W_{mn}^1, W_{mn}^2\right] \cdot \sin\frac{m\pi}{a}x \cdot \sin\frac{n\pi}{b}y. \tag{35}$$

Substituting Eqs. (35) into Eq. (11) will show that the Navier's solution exists only if following coefficients are zero:

$$A_{13} = A_{23} = A_{45} = E_{13} = E_{23} = E_{45} = F_{13} = F_{23} = F_{45} = G_{13} = G_{23} = G_{45} = R_{13} = R_{23} = R_{45},$$
$$B_{13}^I = B_{23}^I = B_{45}^I = H_{13}^I = H_{23}^I = H_{45}^I = L_{13}^I = L_{23}^I = L_{45}^I = D_{13}^{II} = D_{23}^{II} = D_{45}^{II} = 0, \tag{36}$$

i.e. for the cross ply rectangular laminate composite plates.

Following the standard Navier's procedure, a set of homogenous linear algebraic equations for thermal buckling of rectangular cross-ply laminated plates are obtained:

$$([\boldsymbol{C}] - \Delta T_{cr}[\boldsymbol{G}])\{\boldsymbol{\Delta}\} = \{0\}, \tag{37}$$

where ΔT_{cr} denotes the critical thermal buckling temperature rise. The coefficients of symmetric matrix $[\boldsymbol{C}]$ and $[\boldsymbol{G}]$ are given as follows.

$$c_{11} = -A_{11}\alpha^2 - A_{33}\beta^2, \quad c_{12} = -A_{12}\alpha\beta - A_{33}\alpha\beta,$$
$$c_{14} = -A_{16}\alpha, c_{15} = -2E_{16}\alpha,$$
$$c_{22} = -A_{33}\alpha^2 - A_{22}\beta^2, \quad c_{24} = -A_{26}\beta, \quad c_{25} = -2E_{26}\beta,$$
$$c_{33} = -A_{44}\alpha^2 - A_{55}\beta^2, \quad c_{34} = -E_{44}\alpha^2 - E_{55}\beta^2,$$
$$c_{35} = -F_{44}\alpha^2 - F_{55}\beta^2,$$
$$c_{44} = -F_{44}\alpha^2 - F_{55}\beta^2 + A_{66}, \quad c_{45} = -G_{44}\alpha^2 - G_{55}\beta^2 + 2E_{66},$$
$$c_{55} = -R_{44}\alpha^2 - R_{55}\beta^2 + 4F_{66},$$
$$c_{11}^I = -B_{11}^I\alpha^2 - B_{33}^I\beta^2, \quad c_{12}^I = -B_{12}^I\alpha\beta - B_{33}^I\alpha\beta,$$
$$c_{22}^I = -B_{33}^I\alpha^2 - B_{22}^I\beta^2, \quad c_{31}^I = -B_{44}^I\alpha, \quad c_{32}^I = -B_{55}^I\beta,$$
$$c_{41}^I = H_{44}^I\alpha - B_{16}^I\alpha, \quad c_{42}^I = H_{55}^I\beta - B_{26}^I\beta, \quad c_{51}^I = -2H_{16}^I\alpha + L_{44}^I\alpha,$$
$$c_{52}^I = -2H_{26}^I\beta + L_{55}^I\beta,$$
$$c_{11}^{II} = -D_{11}^{II}\alpha^2 - D_{33}^{II}\beta^2 + D_{44}^{II}, \quad c_{12}^{II} = -D_{12}^{II}\alpha\beta - D_{33}^{II}\alpha\beta + D_{55}^{II},$$
$$c_{22}^{II} = -D_{33}^{II}\alpha^2 - D_{22}^{II}\beta^2 + D_{55}^{II},$$
$$G_{33} = N_{Txx}^0 \cdot \alpha^2 + N_{Tyy}^0 \cdot \beta^2, G_{34} = M_{Txx}^0 \cdot \alpha^2 + M_{Tyy}^0 \cdot \beta^2,$$
$$G_{35} = R_{Txx}^0 \cdot \alpha^2 + R_{Tyy}^0 \cdot \beta^2, G_{44} = R_{Txx}^0 \cdot \alpha^2 + R_{Tyy}^0 \cdot \beta^2,$$
$$G_{45} = S_{Txx}^0 \cdot \alpha^2 + S_{Tyy}^0 \cdot \beta^2, G_{55} = P_{Txx}^0 \cdot \alpha^2 + P_{Tyy}^0 \cdot \beta^2,$$
$$G_{IJ} = 0 \text{ otherwise}. \tag{38}$$

where $\alpha = \frac{m\pi}{a}$, $\beta = \frac{n\pi}{b}$.

Solution of equations (37) give for each choice of (m,n) the characteristic numbers or eigenvalues ΔT_{mn}. The smallest of all ΔT_{mn} not equal to zero is the critical buckling temperature ΔT_{cr}. The eigenvector of buckling mode shapes is then $\{\boldsymbol{\Delta}\} = \{\, u_{0mn} \quad v_{0mn} \quad W_{mn}^0 \quad W_{mn}^1 \quad W_{mn}^2 \quad U_{mn}^I \quad V_{mn}^I \,\}^T$.

4.2. Analytical solution of the LW Theory of Reddy

Navier's solution of the LW Theory of Reddy is derived for the rectangular cross-ply laminated plates *axb* with the following simply supported boundary conditions:

$$v_0 = w_0 = V^I = N_{xx} = N_{xx}^I = 0 \quad \text{at} \quad x = 0,\ a,$$
$$u_0 = w_0 = U^I = N_{yy} = N_{yy}^I = 0 \quad \text{at} \quad y = 0,\ b. \tag{39}$$

The displacement field which satisfies the boundary conditions (39) and Euler–Lagrange equilibrium equations (17), is given in the form:

$$\left[u_o(x,y); U^I(x,y)\right] = \sum_{m=1}^{\infty}\sum_{n=1}^{\infty}\left[u_{0mn}; U_{mn}^I\right] \cdot \cos\frac{m\pi}{a}x \cdot \sin\frac{n\pi}{b}y,$$

$$\left[v_0(x,y); V^I(x,y)\right] = \sum_{m=1}^{\infty}\sum_{n=1}^{\infty}\left(v_{0mn}; V_{mn}^I\right) \cdot \sin\frac{m\pi}{a}x \cdot \cos\frac{n\pi}{b}y,$$

$$w_0(x,y) = \sum_{m=1}^{\infty}\sum_{n=1}^{\infty} W_{mn}^0 \cdot \sin\frac{m\pi}{a}x \cdot \sin\frac{n\pi}{b}y. \tag{40}$$

Substituting Eqs. (40) into Eq. (17) will show that the Navier's solution exists only if following coefficients are zero:

$$A_{13} = A_{23} = A_{45} = B_{13}^I = B_{23}^I = B_{45}^I = D_{13}^{II} = D_{23}^{II} = D_{45}^{II} = 0, \tag{41}$$

i.e. for the cross ply rectangular laminate composite plates.

Following the standard Navier's procedure, a set of homogenous linear algebraic equations for thermal buckling of rectangular cross-ply laminated plates are obtained:

$$([\boldsymbol{C}] - \Delta T_{\boldsymbol{cr}}[\boldsymbol{G}])\{\boldsymbol{\Delta}\} = \{\boldsymbol{0}\}, \tag{42}$$

where $[\boldsymbol{C}]$ is given in [52], while matrix $[\boldsymbol{G}]$ is:

$$[\boldsymbol{G}]=\begin{bmatrix} 0 & 0 & 0 & 0 & 0 \\ & 0 & 0 & 0 & 0 \\ & & {}^{33}G & 0 & 0 \\ & sym. & & 0 & 0 \\ & & & & 0 \end{bmatrix}, \quad \text{where} \quad {}^{33}G=\left(N^0_{Txx}\cdot\alpha^2+N^0_{Tyy}\cdot\beta^2\right), \tag{43}$$

while $\alpha=\frac{m\pi}{a}$, $\beta=\frac{n\pi}{b}$.

Solution of equations (42) give for each choice of (m,n) the characteristic numbers or eigenvalues ΔT_{mn}. The smallest of all ΔT_{mn} not equal to zero is the critical buckling temperature ΔT_{cr}. The eigenvector of buckling mode shapes is then $\{\Delta\}=\{\,u_{0mn}\quad v_{0mn}\quad W^0_{mn}\quad U^I_{mn}\quad V^I_{mn}\,\}^T$.

5. Numerical results and discussion

Using previous derived finite element and analytical solutions of the LW Theory of Reddy, an original computer program was coded using MATLAB programming language, for thermal buckling of laminated composite plates. Element stiffness matrix and element geometric stiffness matrix were evaluated using 3×3 Gauss–Legendre integration scheme for 2D quadratic in-plane interpolation. The parametric effect of temperature distribution, side-to-thickness ration a/h, plate aspect ratio a/b, modulus ratio E_1/E_2 and thermal expansion coefficient ratio α_2/α_1, as well as boundary conditions on critical buckling temperature of laminated composite plates are analyzed. The following boundary conditions at the plate edges are used:Simply supported:

$$\textbf{SSSS}: \quad \begin{cases} x=0,\ a: & v_0=w_0=V^I=0 \\ y=0,\ b: & u_0=w_0=U^I=0 \end{cases} \quad I=1,\ldots N+1, \tag{44}$$

Clamped:

$$\textbf{CCCC}: \quad \begin{cases} x=0,a: & u_0=v_0=w_0=U^I=V^I=0 \\ y=0,b: & u_0=v_0=w_0=U^I=V^I=0 \end{cases} \quad I=1,\ldots N+1. \tag{45}$$

The accuracy of the present formulation is demonstrated through a number of examples and by comparison with results available in the literature. Some new results are also presented.

Example 5.1. In order establish the accuracy of the present theory, as a first example an isotropic $((a/h=100,\ a/b=1,\ \alpha=2x10^{-6},\ v=0.30))$ thin $(a/h=100)$ square plate with simply supported or clamped edges, subjected to uniform $\Delta T_{cr}=\Delta T_{cr}$ or linearly varying $\Delta T_{cr}=\frac{\Delta T_{cr}}{h}\cdot z$ temperature rise is analyzed. Table 1 shows that the present model is in a good agreement with CLPT [54], FSDT [20,28,55] and LW [43] models from the literature. The critical temperature obtained for the case of linearly varying temperature distribution is double the critical temperatures for the uniform temperature distribution. This is because the thermal stress resultant of the linearly varying temperature case is half of the uniform temperature case. Also, it can be seen that the critical temperatures of clamped plate are higher than for the simply supported plate. The reason for this may be the enhanced stiffness of the laminate imposed by clamped edges.

Table 2
Critical temperature $\Delta\overline{T}_{cr}$ of isotropic plate for different a/h ratios and uniform temperature rise $(E=1,\ \alpha=1\times10^{-6},\ v=0.30,\ a/b=1)$.

a/h	Present	3D [48]	HSDT [41]	HSDT [57]
Isotropic				
2	0.1201	/	0.1253	/
10/3	0.7419×10^{-1}	0.7193×10^{-1}	0.7193×10^{-1}	/
4	0.5853×10^{-1}	0.5600×10^{-1}	0.5600×10^{-1}	0.5860×10^{-1}
5	0.4138×10^{-1}	0.3990×10^{-1}	0.3990×10^{-1}	0.4134×10^{-1}
20/3	0.2529×10^{-1}	0.2468×10^{-1}	0.2468×10^{-1}	/
10	0.1198×10^{-1}	0.1183×10^{-1}	0.1183×10^{-1}	0.1198×10^{-1}
20	0.3120×10^{-2}	0.3109×10^{-2}	0.3109×10^{-2}	0.3120×10^{-2}
100	0.1265×10^{-3}	0.1264×10^{-3}	0.1264×10^{-3}	0.1256×10^{-3}

Table 3
Critical temperature $\Delta\overline{T}_{cr}$ of isotropic plate for different a/b ratios and uniform temperature rise $(E=1,\ \alpha=1\times10^{-6}\ 1/^{\circ}C,\ v=0.30,\ a/h=100)$.

a/b	Present	FSDT [56]	CLPT [54]	FSDT [15]
Isotropic				
0.25	0.6791	0.6727	0.6722	0.691
0.50	0.7970	0.7913	0.7908	0.814
0.75	0.9946	0.9890	/	/
1.0	1.2650	1.2657	1.2653	1.319
1.25	1.6300	1.6234	/	/
1.50	2.0675	2.0561	2.0562	2.101
1.75	2.5843	2.5696	/	/
2.0	3.1802	3.1617	3.1633	3.191
2.25	3.8549	3.8324	/	/
2.50	4.6080	4.5817	4.5868	4.601
2.75	5.4393	5.4096	/	/
3.0	6.3487	6.3144	6.3267	6.330

Example 5.2. An isotropic $(E=1,\ \alpha=1\times10^{-6},\ v=0.30)$ simply supported plate subjected to uniform temperature rise is analyzed by varying geometric parameters, such as plate to thickness ratio a/h and plate aspect ratio a/b. The critical temperature is normalized in the following form $\Delta\overline{T}_{cr}=\alpha\Delta T_{cr}$ in Table 2, or as $\Delta\overline{T}_{cr}=\alpha\Delta T_{cr}10^{-4}$ is Table 3. Table 2 shows that the critical temperatures of the present model are in good agreement with 3D [48] and HSDT [41,57] models from the literature for all side to thickness ratios a/h. The results show that the rigidity and thus the critical temperature decrease as the plate thickness ratio increases. Table 3 shows the variation of critical temperature with aspect ratio a/b and $a/h=100$. Again a very good agreement of the present model with CLPT [54] and FSDT [56,15] models from the literature is achieved. As expected, plate geometry, given as a/b ratio, has significant influence on critical temperature. With the increase of a/b ratio, critical temperature increase nonlinearly, up to approximately $a/b<2$. After that, further increase in a/b ratio, gives almost linearly increase of critical temperature. More specially, for $a/b>2$ there is no change of the buckling mode shape with the variation of aspect ratio, since the curve goes up smoothly without any cusp. Finally, Table 4 presents the convergence analysis of thermal buckling loads predicted by the present formulation and tree different plate theories, which are FSDT [69], HSDT [41] and 3D [48]. In wish to justify the Koiter's recommendation, so

Table 1
Critical temperature $\Delta\overline{T}_{cr}$ of isotropic plate subjected to different forms of temperature distributions and boundary conditions $(a/h=100,\ a/b=1,\ \alpha=2\times10^{-6},\ v=0.30)$.

BC	Temperature rise	Present	FSDT [28]	CLPT [54]	FSDT [55]	FSDT [20]	LW [43]
Isotropic							
SS	Uniform	63.2	63.3	63.3	63.3	63.2	62.1
	Linearly varying	126.5	/	126.0	/	/	/
CC	Uniform	173.483	168.0	167.7	167.9	169.1	166.9
	Linearly varying	347.0	/	332.5	/	/	/

Table 4
Convergence of critical temperature $\Delta\overline{T}_{cr}$ of isotropic simply supported plate under a uniform temperature rise ($E=1,\ \alpha=1\times10^{-6},\ \nu=0.30,\ a/b=1,\ a/h=10$).

a/h	Present $n_x\cdot n_y\cdot m$	FSDT [69]	3D [48]	HSDT [41]	$n_x\cdot n_y$			
	$4\times4\times1$	$4\times4\times5$			$4\times4\times10$	16×16	18×18	20×20
Isotropic								
10	0.1209×10^{-1}	0.1200×10^{-1}	0.1198×10^{-1}	0.1201×10^{-1}	0.1200×10^{-1}	0.1199×10^{-1}	0.1183×10^{-1}	0.1183×10^{-1}
20	0.3127×10^{-2}	0.3121×10^{-2}	0.3120×10^{-2}	0.3082×10^{-2}	0.3085×10^{-2}	0.3089×10^{-2}	0.3109×10^{-2}	0.3109×10^{-2}
100	0.1265×10^{-3}	0.1265×10^{-3}	0.1265×10^{-3}	0.1284×10^{-3}	0.1273×10^{-2}	0.1271×10^{-2}	0.1264×10^{-3}	0.1264×10^{-3}

Table 5
Convergence of critical temperature $\Delta\overline{T}_{cr}$ of isotropic ceramic plate for different a/h ratios and temperature rises ($E=380\ GPa,\ \alpha=1\times10^{-6}\ 1/^{\circ}C,\ \nu=0.30,\ a/b=1$).

	Theory		a/h					
			10	20	40	60	80	100
Isotropic								
	CLPT [61]		1709.911	427.477	106.869	47.497	26.717	17.099
	FSDT [64]		1593.902	419.739	106.370	47.396	26.684	17.084
	HSDT [61]		1617.484	421.516	106.492	47.424	26.693	17.088
	HSDT [62]		1599.294	420.146	106.404	47.405	26.688	17.087
Uniform	EDZ_{888} [67]		1599.294	420.146	106.404	47.405	26.688	17.087
	EDZ_{333} [67]		1599.322	420.146	106.404	47.410	26.691	17.087
	ED_{999} [67]		1599.293	420.146	106.404	47.405	26.688	17.087
	ED_{444} [67]		1599.294	420.146	106.404	47.405	26.688	17.087
	ED_{222} [67]		1609.305	420.844	106.449	47.414	26.691	17.088
	Present	$m=2$	1633.155	422.513	106.556	47.436	26.698	17.091
		$m=10$	1619.396	421.584	106.497	47.423	26.694	17.089
	CLPT [61]		3409.821	844.955	203.738	84.995	43.434	24.198
	FSDT [64]		/	/	/	/	/	/
	HSDT [61]		3224.968	833.032	202.984	84.848	43.387	24.177
	HSDT [62]		/	/	/	/	/	/
Linear	EDZ_{888} [67]		3188.250	830.287	202.808	84.812	43.377	24.172
	EDZ_{333} [67]		3188.308	830.287	202.808	84.810	43.375	14.172
	ED_{999} [67]		3188.250	830.286	202.808	84.811	43.476	24.174
	ED_{444} [67]		3188.250	830.286	202.808	84.811	43.376	24.174
	ED_{222} [67]		3208.314	831.684	202.898	84.829	43.382	24.177
	Present	$m=2$	3266.311	845.027	213.113	94.871	53.395	34.182
		$m=10$	3238. 927	843.167	212.994	94.848	53.388	34.179

called h-refinement [71], or through the thickness refinement of in-plane displacements (u,v), denoted as m-number of subdivisions through the thickness, is applied for the present model. As expected, the present results shows that the through the thickness refinement has more influence on the response of thick compare to thin plates. A very close agreement is obtained with 3D and HSDT [41] models in which transverse normal strain assumption is included, compared to FSDT [69] model, which neglects it.

Example 5.3. An isotropic ceramic ($E=380\,\text{GPa}, \alpha=7.4\times10^{-6}\ 1/^{\circ}\text{C}, \nu=0.30$) simply supported plate subjected to uniform $\Delta T_{cr}=\Delta T_{cr}$ or linearly varying $\Delta T_{cr}=\frac{\Delta T_{cr}}{h}\cdot z$ temperature rise is analyzed. The critical temperature is normalized in the following form $\Delta\overline{T}_{cr}=\Delta T_{cr}$ in Table 5, and is given for different of plate thicknesses. The Koiter's recommendation is again verified by the fact that increasing the number of subdivisions $m>1$ through the thickness gives better results, especially for thick plates. For thick plates closer agreement is obtained with the results of CUF based theories, such as ESL or Zig-Zag [67], where transverse normal deformation or at least transverse shear deformation [62,64] is included into a model. The statement verified in the Example 5.1, that the linearly varying temperature distribution is double the critical temperatures for the uniform temperature distribution, is violated when ceramic isotropic plate is analyzed as FGM plate [61,62,64,67] in case of very thin plates. Fig. 3 shows critical temperature of thin ceramic plate ($a/h=100$) for different aspect ratio a/b and different boundary conditions. A close agreement with the results of CPT [62,65] from the literature is achieved.

Example 5.4. A critical temperature of orthotropic simply supported square plate ($a/b=1$) subjected to uniform temperature rise is analyzed. Material constants are given as:

$$E_L/E_T=15, quad E_T=1\ \text{GPa},\quad G_{LT}/E_T=0.5,\quad G_{TT}/E_T=0.3356,$$
$$\nu_{LT}=0.30,\quad \nu_{TT}=0.49,\quad \alpha_L/\alpha_0=0.015,\quad \alpha_T/\alpha_0=1.$$

The critical temperature is normalized in the following form $\Delta\overline{T}_{cr}=\alpha_0\Delta T_{cr}$. Table 6 presents the effect of side to thickness ratio a/h on non-dimensional critical temperature $\Delta\overline{T}_{cr}$ corresponding to (1,2) buckling mode. The present model shows excellent agreement with 3D [48] and HSDT [41,57] models from the literature. As in the previous example decrease of plate stiffness with the decrease of a/h ratio, decrease the critical temperature. The decrease of critical temperature is faster for thick, compared to thin plates. Very close agreement is obtained with the results of HSDT [41,57] and 3D [48] elasticity theory.

Example 5.5. A critical temperature of cross-ply 0/90 simply supported square plate ($a/b=1$) subjected to uniform temperature rise is analyzed. Material constants are given as:

$$E_L/E_T=15,\ \ E_T=1\,\text{GPa},\ \ G_{LT}/E_T=0.5,\ \ G_{TT}/E_T=0.3356,$$
$$\nu_{LT}=0.30,\ \ \nu_{TT}=0.49,\ \ \alpha_L/\alpha_0=0.015,\ \ \alpha_T/\alpha_0=1,\ \ \alpha_0=10^{-6}.$$

The critical temperature is normalized in the following form $\Delta\overline{T}_{cr}=\alpha_0\Delta T_{cr}$. Table 7 presents the effects of side to thickness ratio a/h on non-dimensional critical temperature $\Delta\overline{T}_{cr}$ corresponding to (1,1) buckling mode. Koiter's recommendation is justified using 'm'

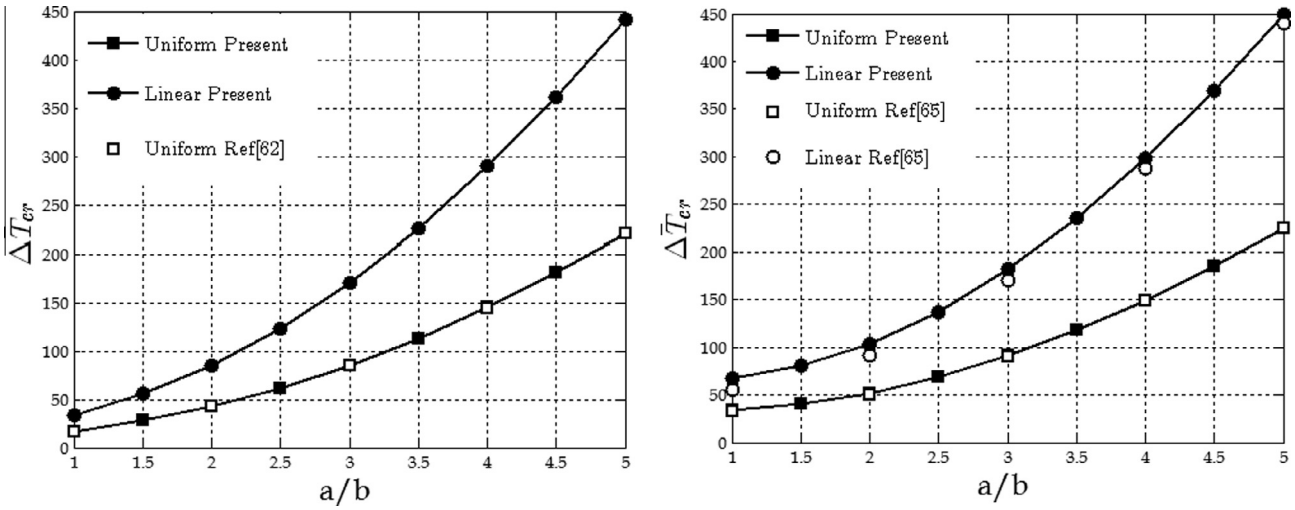

Fig. 3. Effect of a/b ratio of thin ($a/h = 100$) isotropic ceramic plate with (a) SSSS and (b) SCSC boundary conditions on critical buckling temperature $\Delta\bar{T}_{cr}$.

Table 6
Critical temperature $\Delta\bar{T}_{cr}$ of orthotropic plate for different a/h ratios and uniform temperature rise.

a/h	Present	3D [48]	HSDT [41]	HSDT [57]
Orthotropic				
2	0.2875	/	0.2761	/
10/3	0.2162	0.2057	0.2057	/
4	0.1868	0.1777	0.1777	0.1878
5	0.1504	0.1436	0.1436	0.1506
20/3	0.1069	0.1029	0.1029	/
10	0.5923×10^{-1}	0.5782×10^{-1}	0.5782×10^{-1}	0.5918×10^{-1}
20	0.1753×10^{-1}	0.1739×10^{-1}	0.1739×10^{-1}	0.1752×10^{-1}
100	0.7466×10^{-3}	0.7463×10^{-3}	0.7463×10^{-3}	0.7463×10^{-3}

subdivisions through the plate thickness. Increasing the number of subdivisions, plate becomes more flexible and lower values of critical buckling temperature is obtained, especially for thick laminates, thus approaching to values of *M*th order higher deformation theory from the literature [41], in which transverse normal strain is included.

Example 5.6. A critical temperature of cross-ply 0/90/0 plate with simply supported or clamped edges subjected to uniform temperature rise is analyzed. Material constants are given as:

$$E_L/E_T = 15, \quad E_T = 1\ \text{GPa}, \quad G_{LT}/E_T = 0.5, \quad G_{TT}/E_T = 0.3356,$$
$$\nu_{LT} = 0.30, \quad \nu_{TT} = 0.49, \quad \alpha_L/\alpha_0 = 0.015, \quad \alpha_T/\alpha_0 = 1,$$
$$\alpha_0 = 10^{-6}.$$

The critical temperature is normalized in the following form $\Delta\bar{T}_{cr} = \alpha_0 \Delta T_{cr}$. Table 8 presents the convergence analysis of non-dimensional critical temperature $\Delta\bar{T}_{cr}$ of simply supported square plate for different side to thickness ratio a/h. Like in the previous example, Koiter's recommendation is justified by applying convergence analysis in the thickness direction using *m*-subdivisions within each material layer. The *h*-refinement leads to close agreement with 3D [48] and HSDT [41,57] models from the literature, for moderately thick to thin laminates. It may be assumed that better convergence characteristics for thick laminates may be obtained using higher order expansion on transverse displacement through the thickness, as proposed by the presently derived new version of LW Theory of Reddy. After establishing the accuracy of

Table 7
Convergence of critical $\Delta\bar{T}_{cr}$ of cross-ply 0/90 plate for different a/h ratios and uniform temperature rise.

Theory	*m*	*a/h*							
		2	10/3	4	5	20/3	10	20	100
Laminate [0/90]									
Present	1	0.3695	0.2391	0.1926	0.1419	0.9052×10^{-1}	0.4449×10^{-1}	0.1188×10^{-1}	0.4858×10^{-3}
	5	0.3422	0.2263	0.1841	0.1372	0.8856×10^{-1}	0.4401×10^{-1}	0.1184×10^{-1}	0.4857×10^{-3}
	10	0.3398	0.2252	0.1834	0.1367	0.8838×10^{-1}	0.4397×10^{-1}	0.1184×10^{-1}	0.4857×10^{-3}
HSDT [41]		0.3198	0.2114	0.1729	0.1302	0.8524×10^{-1}	0.4310×10^{-1}	0.1177×10^{-1}	0.4856×10^{-3}

Table 8
Convergence of critical temperature $\Delta\bar{T}_{cr}$ of cross-ply 0/90/0 plate for different a/h ratios and uniform temperature rise.

Theory	*m*	*a/h*							
		2	10/3	4	5	20/3	10	20	100
Laminate [0/90/0]									
Present	1	0.3595	0.2625	0.2272	0.1848	0.1340	0.7628×10^{-1}	0.2316×10^{-1}	0.9964×10^{-3}
	5	0.3429	0.2518	0.2185	0.1786	0.1305	0.7502×10^{-1}	0.2303×10^{-1}	0.9961×10^{-3}
	10	0.3418	0.2513	0.2181	0.1784	0.1303	0.7498×10^{-1}	0.2303×10^{-1}	0.9961×10^{-3}
3D [48]		/	/	0.2140	0.1763	/	0.7467×10^{-1}	0.2308×10^{-1}	0.9961×10^{-3}
HSDT [41]		0.3298	0.2447	0.2133	0.1752	0.1287	0.7442×10^{-1}	0.2297×10^{-1}	0.9960×10^{-3}
HSDT [57]		/	/	0.2253	0.1828	/	0.7433×10^{-1}	0.2308×10^{-1}	0.9917×10^{-3}

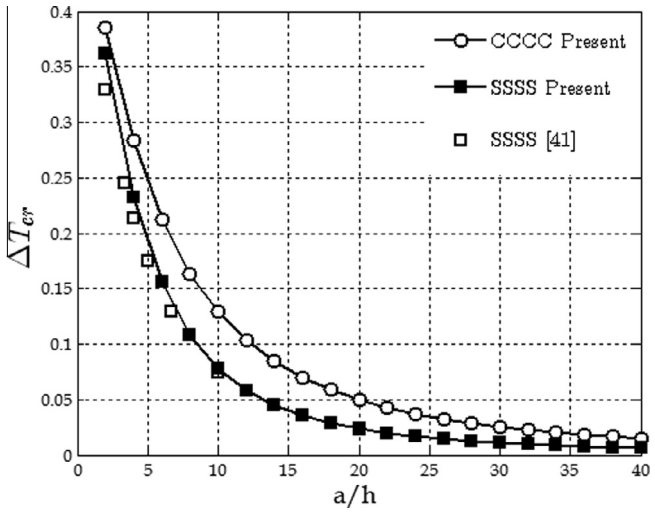

Fig. 4. Effect of a/h ratio of cross-ply 0/90/0 plate on critical buckling temperature $\Delta\bar{T}_{cr}$.

the present model for simply supported edges, effect of boundary conditions on critical temperatures is further investigated. Fig. 4 shows variation of critical temperatures for clamped and simply supported edges as a function of side to thickness ratio a/h. As already mentioned in Example 5.1, clamped edges enhance the plate stiffness, compared to simply supported edges, thus giving higher values of critical temperature. Fig. 5a presents the effects of modulus ratio E_1/E_2 on non-dimensional critical temperatures of plates with clamped and simply supported boundary conditions ($a/h = 10$, $a/b = 1$). It may be seen that with the increase of degree of orthotropy critical temperatures increases, and is greater for plate with clamped edges. However this increase is much faster for simply supported edges, which show more sensitivity to the change of material orthotropy. Fig. 5b presents the effects of thermal expansion coefficient ratio α_2/α_1 on non-dimensional critical temperature of square ($a/b = 1$) laminated plates with different plate thicknesses, i.e. side to thickness ratio a/h. In the present analysis α_2 was varied while α_1 was left constant. The results show that the critical temperature decrease with the increase of α_2/α_1 ratio for all plate thicknesses. Moreover, this decrease of critical temperature is greater for thick, compared to thin laminates. Fig. 6a further analyzes the influence of boundary conditions on critical temperature versus a/b ratio of thick ($a/h = 10$) composite plate. As expected the clamped edges, compared to simply support edges, give higher values of critical temperatures for all a/b ratios. Fig. 6b shows the influence of a/b ratio on critical temperatures for square simply supported plate with various plate thicknesses,

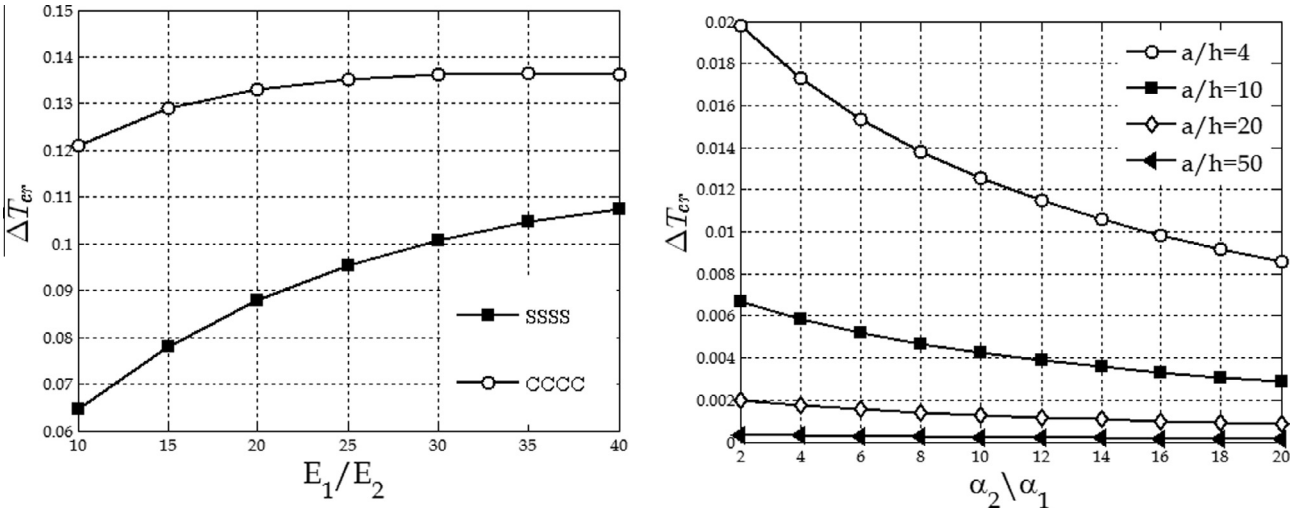

Fig. 5. Effect of E_1/E_2 and α_2/α_1 ratio of cross-ply 0/90/0 plate on critical buckling temperature $\Delta\bar{T}_{cr}$.

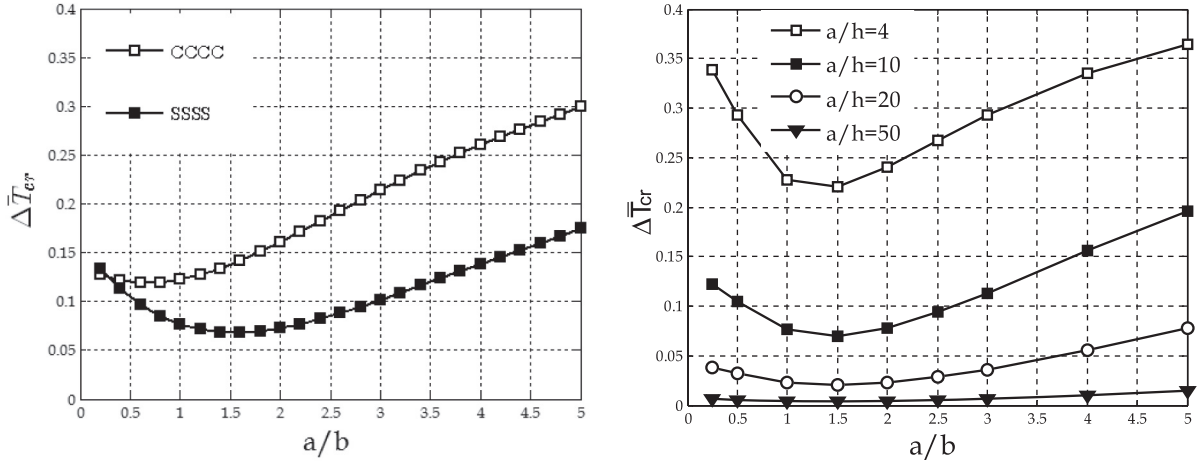

Fig. 6. Effect of a/b ratio of cross-ply 0/90/0 plate on critical buckling temperature $\Delta\bar{T}_{cr}$ for different (a) boundary conditions and (b) plate thickness.

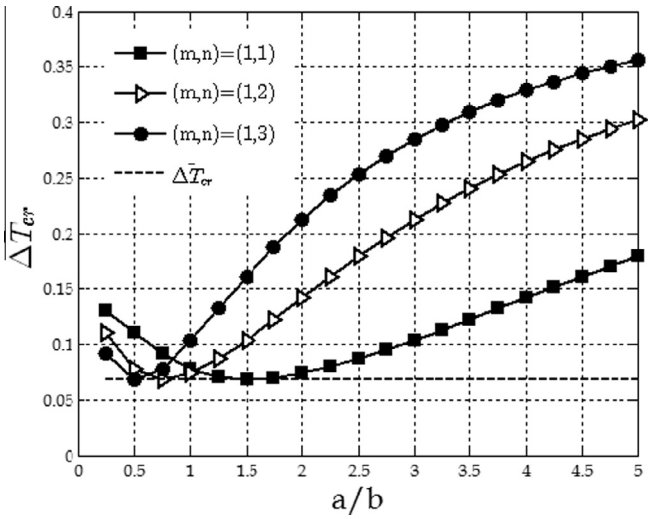

Fig. 7. Effect of a/b ratio of cross-ply 0/90/0 plate on critical buckling temperature $\Delta\bar{T}_{cr}$ for different mode shapes ($a/h = 10$).

given as a/h ratio. Unlike in the case of thin isotropic plate in Example 5.2, which shows monotonic increase of critical temperature with a/b ratio, response of thick ($a/h < 20$) 0/90/0 cross-ply plate posses a concavity. Namely, for $a/b < 1.5$ critical temperature shows monotonic decrease, attaining minimum at $a/b = 1.5$. For further increase of $a/b > 1.5$ critical temperature shows monotonic increase with a/b ratio. The cusp at $a/b = 1.5$ may imply that there will be a change in buckling mode shape, with the change of a/b ratio. This is verified on Fig. 7, which shows that as the width of the plate increases, by leaving the constant length, critical temperature is obtained at higher modes. However, this dependence of critical temperature with a/b ratio becomes of no importance after the third mode (1,3). Fig. 8 shows first three buckling modes of thick ($a/h = 10$) rectangular ($a/b = 1.5$) simply supported laminated plate.

Example 5.7. A critical temperature of cross-ply 0/90/90/0 with simply supported or clamped edges subjected to uniform temperature rise is analyzed. Material constants are given as:Material (1):

$$E_1/E_2 = 25, \quad G_{12}/E_2 = 0.5, \quad G_{13}/E_2 = 0.5, \quad G_{23}/E_2 = 0.2,$$
$$\nu_{12} = \nu_{13} = \nu_{23} = 0.25, \quad \alpha_2/\alpha_1 = 3, \quad \alpha_1 = 1.$$

Material (2):

$$E_1/E_2 = 20, \quad G_{12}/E_2 = G_{13}/E_2 = G_{23}/E_2 = 0.50,$$
$$\nu_{12} = \nu_{13} = \nu_{23} = 0.25, \quad \alpha_2/\alpha_1 = 2, \quad \alpha_1 = 0.1 \cdot 10^{-5}\ 1/^{\circ}\mathrm{C}.$$

The critical temperature is normalized in the following form $\Delta\overline{T}_{cr} = \frac{a^2 h}{\pi^2 D_{22}}\Delta T_{cr}$ in Table 7 for Material (1), or as $\Delta\overline{T}_{cr} = \alpha_1 \Delta T_{cr} 10^4$ on Fig. 9 for Material (2). Table 9 presents the effects of side to thickness ratio a/h on non-dimensional critical temperature $\Delta\overline{T}_{cr}$

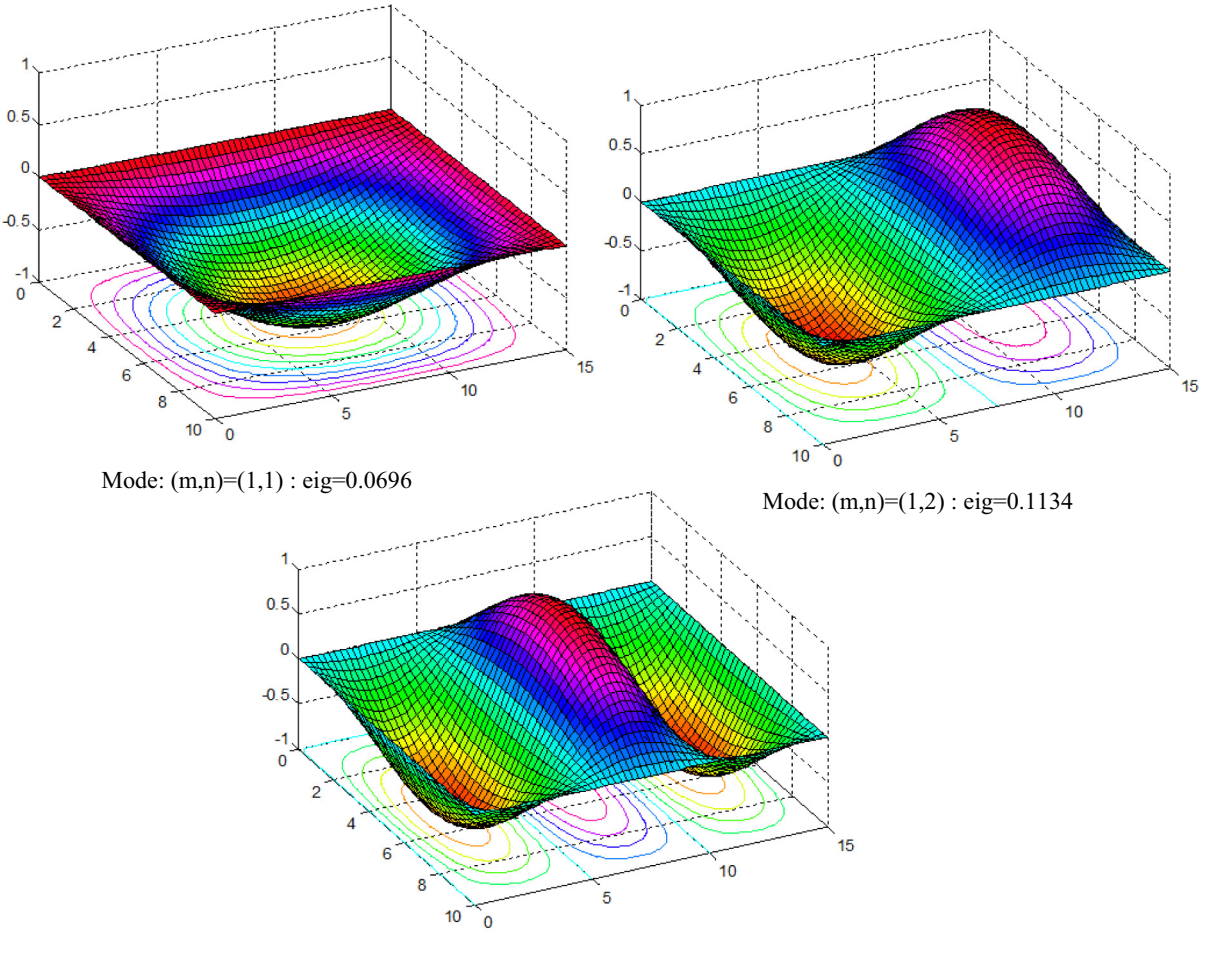

Fig. 8. Buckling mode shapes of cross-ply 0/90/0 simply supported square plate ($a/b = 1.5$, $a/h = 10$).

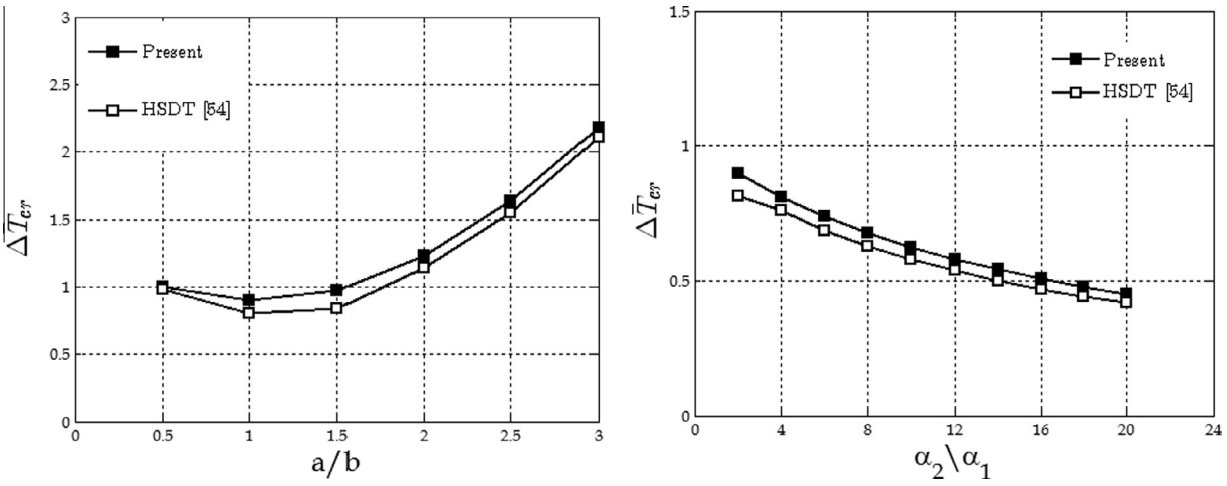

Fig. 9. Effect of a/b and α_2/α_1 ratio of cross-ply 0/90/90/0 plate on critical buckling temperature $\Delta\bar{T}_{cr}$.

Table 9
Critical temperature $\Delta\bar{T}_{cr}$ of cross-ply 0/90/90/0 plate for different a/h ratios and uniform temperature rise.

a/h	Present	FSDT [60]	HSDT [57]	HSDT [35]	RPT [66]	GRT [66]		
						$p = 3$ (TOT)	$p = 5$	$p = 7$
Laminate [0/90/90/0]								
4	0.0514	0.0613	0.0570	0.0554	0.07115	0.05580	0.05888	0.06109
10	0.1400	0.1598	0.1479	0.1436	0.17492	0.14784	0.15344	0.15704
20	0.1976	/	0.2088	/	/	/	/	/
50	0.2245	/	0.2383	/	/	/	/	/
100	0.2291	0.2438	0.2432	0.2431	0.24405	0.24331	0.24378	0.24359
1000	0.2306	/	/	0.2450	0.24510	0.24502	0.24516	0.24502

of simply supported square plate. The present model shows closer agreement with HSDT [57,35] models, than with FSDT [60], RPT [66] and GRT [66] for $p = 7$ models, especially for thick laminates. This may be due to assumptions placed on transverse shear stress distribution as well as the fact that the interpolation functions with orders higher than 3, may lead to oscillatory or uncontrolled results [66]. Namely, the continuity conditions of transverse shear stresses across each layer interface, as well as stress free boundary condition on plate interfaces, are satisfied in present and HSDT model, while FSDT model does not satisfy the second condition, due to assumption of constant transverse shear stresses across the plate thickness. Unlike in previously analyzed plate models, this lamination scheme shows the increase of critical temperature with the decrease of plate thickness, becoming for $a/h > 40$ almost constant.

Fig. 9a shows variation of critical temperature with a/b ratio for thin $a/h = 100$ simply supported square plate with Material (2). Results of the present model are compared with HSDT [54] model from the literature and close agreement is achieved. Like in the previous examples, critical temperature shows almost monotonic increase with the increase of a/b ratio, after attaining its minimum value for $a/b = 1$. The effect of degree of thermal orthotropy, given as ratio of linear thermal expansion coefficient α_2/α_1, on critical temperature is shown on Fig. 9b. Results from the present model are compared with HSDT [54] model from the literature and close agreement is achieved. Like in the Example 5.5, as the ratio α_2/α_1 increases the critical temperature decreases.

6. Conclusion

In this paper the finite element and closed form solution are derived for the thermal buckling analysis of laminated composite plates using Generalized Layerwise Plate Theory (GLPT) of Reddy and the new version of LW Theory of Reddy. An original MATLAB computer programs, coded for both the finite element and closed form solution of GLPT are used to study effects of various parameters on critical buckling temperature of laminated composite plates and the following conclusions may be derived:

1. By increasing the number of subdivisions through the plate thickness, or using so called h-refinement, through the thickness refinement of in-plane displacements (u,v) may be modeled, which is especially important for thick laminates in thermal environment. However, better results for thick laminates may be expected by using higher order expansion of transverse displacement through the thickness, as given in the present new version of LW Theory of Reddy.
2. The critical buckling temperature under the linear temperature rise is higher, than under the uniform temperature rise.
3. The critical buckling temperature for clamped boundary conditions is higher than for simply supported boundary conditions.
4. Depending on lamination scheme the critical buckling temperature shows monotonic response with side to thickness ratio a/h. This increase/decrease is faster for thick $a/h < 20$ laminates, compared to thin laminates.
5. The critical buckling temperature increases with the increase of aspect ratio a/b. This increase is again more pronounced for thick, compared to thin laminates, and for clamped compared to simply supported edges. For $a/b > 2$ the increase of critical temperature is almost linear, and thus the same for all buckling mode shapes.
6. The critical buckling temperature increases with the increase of modulus ratio E_1/E_2.

7. The critical buckling temperature decreases with the increase of thermal expansion coefficient ratio α_2/α_1 and is faster for thick, compared to thin laminates.
8. The critical buckling temperature depend on the lamination scheme, especially for thick laminates and is greater for [0/90/0], compared to [0/90], compared to [0] laminates, when the same material properties of each layer are used.

Finally, it may be concluded that the thick laminates show more sensitivity to thermal buckling with the change of plate geometry and material orthotropy, compared to thin laminates, the reason why refined plate theories, such as layerwise plate theories, should be used. Furthermore, transverse normal strain cannot be discarder especially for thick laminates in thermal environment.

Acknowledgement

The author is thankful for the financial support received by the Ministry of Education and Science of the Republic of Serbia, Project TP 36048.

References

[1] Gossard ML, Seide P, Roberts WM. Thermal buckling of plates. NACA TND 2771; 1952.
[2] Klosner JM, Forray MI. Buckling of simply supported plates under arbitrary symmetrical temperature distribution. J Aeronaut Sci 1958;25:181–4.
[3] Miura K. Thermal buckling of rectangular plates. J Aerosp Sci 1961;28:341–2.
[4] Gowda RMS, Pandalai KAV. Thermal buckling of orthotropic plates. In: Paandalai KAV, editor. Studies in structural mechanics. Madras; 1970. p. 9–44.
[5] Whitney JM, Ashton JE. Effect of environment on the elastic response of layered composite plate. AIAA J 1971;7:1708–13.
[6] Prabhu MSS, Durvasula S. Thermal buckling of restrained skew plates. J Eng Mech ASCE 1974;100:1292–5.
[7] Jones RM. Mechanics of composite materials. New York: McGraw-Hill; 1975.
[8] Tauchert TR, Huang NN. Thermal buckling of symmetric angle-ply laminated plates. In: Marshall IH, editor. Proceedings of the 4th international conference on composite structures. Barking: Elsevier Applied Science Publishers; 1987. p. 1424–35.
[9] Chen LN, Chen LY. Thermal buckling of laminated cylindrical plates. Compos Struct 1987;8:189–205.
[10] Chen LW, Chen LY. Thermal buckling analysis of composite laminated plates by the finite element method. J Therm Stresses 1989;12:41–56.
[11] Javaheri R, Eslami MR. Thermal buckling of functionally graded plates. AIAA J 2002;40(1):162–9.
[12] Tauchert TR. Thermal-buckling of thick antisymmetric angle-ply laminates. J Therm Stresses 1987;10:113–24.
[13] Thangaratnam KR, Palaninathan R, Ramachandran J. Thermal buckling of composite laminated plates. Comput Struct 1989;32:1117–24.
[14] Noor AK, Burton WS, Peters JM. Predictor–corrector procedures for stress and free vibration analyses of multilayered composite plates and shells. Comput Mech Eng 1990;82(1–3):341–63.
[15] Chen WJ, Lin PD, Chen LW. Thermal buckling behavior of thick laminated plates under nonuniform temperature distribution. Comput Struct 1991;41(4):637–45.
[16] Mathew TC, Singh G, Rao GV. Thermal buckling of cross-ply composite laminates. Comput Struct 1992;42:281–7.
[17] Huang NN, Tauchert TR. Thermal buckling of clamped symmetric laminated plates. Thin Walled Struct 1992;13:259–73.
[18] Chen WC, Liu WH. Thermal buckling of antisymmetric angle-ply laminated plates – an analytical Levy-type solution. J Therm Stresses 1993;16:401–19.
[19] Ahmed KN, James Jr HS, Jeanne MP. Thermo-mechanical buckling and post buckling of multilayered composite panels. Compos Struct 1993;23:233–51.
[20] Prabhu MR, Dhanaraj R. Thermal buckling of laminated composite plates. Comput Struct 1994;53:1193–204.
[21] Argyris J, Tenek L. High-temperature bending, buckling, and post buckling of laminated composite plates using the natural, mode method. Comput Methods Appl Mech Eng 1994;117:105–42.
[22] Mannini A. Shear deformation effect on thermal buckling of cross-ply composite laminates. Compos Struct 1997;39(1–2):1–10.
[23] Kant T, Babu CS. Thermal buckling analysis of skew fiber reinforced composite and sandwich plates using shear deformable finite element models. Compos Struct 2000;49(1):77–85.
[24] Singha MK, Ramachandra LS, Bandyopadhyay JN. Thermal post buckling analysis of laminated composite plates. Compos Struct J 2001;54:453–8.
[25] Kabir HRH, Askar H, Chaudhuri RA. Thermal buckling response of shear flexible laminated anisotropic plates using a three-node isoparametric element. Compos Struct 2003;59:173–87.
[26] Wu L. Thermal buckling of a simply supported moderately thick rectangular FGM plate. Compos Struct 2004;64(2):211–8.
[27] Kabir HRH, Hamad MAM, Al-Duaij J, John MJ. Thermal buckling response of all-edge clamped rectangular plates with symmetric angle-ply lamination. Compos Struct 2007;79:148–55.
[28] Bouazza M, Tounsi A, Adda-Bedia EA, Megueni A. Thermo elastic stability analysis of functionally graded plates: an analytical approach. Comput Mater Sci 2010;49:865–70.
[29] Nath Y, Shukla KK. Post-buckling of angle-ply laminated plates under thermal loading. Commun Nonlinear Sci Numer Simul 2001;6(1):1–16.
[30] Sun LX, Hsu TR. Thermal buckling of laminated composite plates with transverse shear deformation. Comput Struct 1990;36(5):883–9.
[31] Chang JS. FEM analysis of buckling and thermal buckling of antisymmetric angle-ply laminates according to transverse shear and normal deformation high order displacement theory. Comput Struct 1990;37(6):925–46.
[32] Chang JS, Leu SY. Thermal buckling analysis of antisymmetric angle-ply laminates based on a higher-order displacement field. Compos Sci Technol 1991;41:109–28.
[33] Rohwer K. Thermal buckling analysis of antisymmetric angle-ply laminates based on a higher-order displacement field. Compos Sci Technol 1992;45:181–2.
[34] Chang JS. A further study on thermal buckling of simply supported antisymmetric angle-ply laminates in a uniform-temperature field. Compos Sci Technol 1992;43:309–15.
[35] Shu XP, Sun LX. Thermo-mechanical buckling of laminated composite plates with higher order transverse shear deformation. Comput Struct 1994;53(1):1–7.
[36] Shen HS. Karman-type equations for a higher-order shear deformation plate theory and its use in the thermal post buckling analysis. Appl Math Mech 1997;18(12):1137–51.
[37] Shen HS. Thermo-mechanical post buckling analysis of imperfect laminated plates using a higher order shear-deformation theory. Comput Struct 1998;66(4):395–409.
[38] Kant T, Babu CS. Thermal buckling analysis of skew fiber reinforced composite and sandwich plates using shear deformable finite element models. Compos Struct 2000;49(1):77–85.
[39] Babu CS, Kant T. Refined higher order finite element models for thermal buckling of laminated composite and sandwich plates. J Therm Stress 2000;23:111–30.
[40] Dafedar JB, Desai YM. Thermo-mechanical buckling of laminated composite plates using mixed higher-order analytical formulation. ASME J Appl Mech 2002;69(11):790–9.
[41] Matsunaga H. Thermal buckling of cross-ply laminated composite and sandwich plates according to a global higher-order deformation theory. Compos Struct 2005;68(4):439–54.
[42] Lee J. Thermally induced buckling of laminated composites by a layerwise theory. Comput Struct 1997;65(6):917–22.
[43] Shariyat M. Thermal buckling analysis of rectangular composite plates with temperature-dependent properties based on a layerwise theory. Thin Walled Struct 2007;45:439–52.
[44] Zhen W, Wanji C. Thermo-mechanical buckling of laminated composite sandwich plates using global–local higher order theory. Int J Mech Sci 2007;49(6):712–21.
[45] Shariyat M. Non-linear dynamic thermo-mechanical buckling analysis of the imperfect sandwich plates based on a generalized three-dimensional high-order global–local plate theory. Compos Struct 2010;92:72–85.
[46] Noor AK, Burton WS. Three-dimensional solutions for the free vibrations and buckling of thermally stressed multilayered angle-ply composite plates. ASME J Appl Mech 1992;59(12):868–77.
[47] Noor AK, Burton WS. Three-dimensional solutions for the thermal buckling and sensitivity derivatives of temperature-sensitive multilayered angle-ply plates. ASME J Appl Mech 1992;59(12):848–56.
[48] Noor AK, Burton WS. Three-dimensional solutions for thermal buckling of multilayered anisotropic plates. J Eng Mech 1992;118(4):683–701.
[49] Cetkovic M. Thermo-mechanical bending of laminated composite and sandwich plates using layerwise displacement model. Compos Struct 2015;125:388–99.
[50] Cetkovic M, Vuksanovic Đ. Large deflection analysis of laminated composite plates using layerwise displacement model. Struct Eng Mech 2011;40(2):257–77.
[51] Cetkovic M, Vuksanovic Đ. Bending, free vibrations and buckling of laminated composite and sandwich plates using a layerwise displacement model. Compos Struct 2009;88(2):219–27.
[52] Cetkovic M. Nonlinear behavior of laminated composite plates [Ph.D Thesis] (in Serbian). Serbia: Faculty of Civil Engineering in Belgrade; 2011.
[53] Reddy JN. Mechanics of laminated composite plates. CRC Press; 1999.
[54] Kari RT, Palaninathan, Ramachandran J. Thermal buckling of composite laminated plates. Comput Struct 1989;32(5):1117–24.
[55] Maloy KS, Ramachandra LS, Bandyopadhyay JN. Thermal post buckling of laminated composite plates. Compos Struct 2001;54:453–8.
[56] Chandrashekhara K. Thermal buckling of laminated plates using a shear flexible finite element. Finite Elem Anal Des 1992;12:51–61.
[57] Singh S, Singh J, Shukla KK. Buckling of laminated composite plates subjected to mechanical and thermal loads using meshless collocations. J Mech Sci Technol 2013;27(2):327–36.

[58] Xiaoping S, Liangxin S. Thermo-mechanical buckling of laminated composite plates with higher-order transverse shear deformation. Comput Struct 1994;53(1):1–7.
[59] Wu Z, Chen W. Thermo-mechanical buckling of Laminated composite and sandwich Plates using global–local higher order theory. Int J Mech Sci 2007;49:712–21.
[60] Shukla KK. Some studies on nonlinear analysis of laminated composite plates subjected to thermo-mechanical loading [Ph.D Thesis]. IIT Delhi; 2001.
[61] Javaheri R, Elsami MR. Thermal buckling of functionally graded plates based on higher order theory. J Therm Stresses 2002;25:603–25.
[62] Matsunaga H. Thermal buckling of functionally graded plates according to a 2D higher-order deformation theory. Compos Struct 2009;90(1):76–86.
[63] Zenkour AM, Sobhy M. Thermal buckling of various types of FGM sandwich plates. Compos Struct 2010;93(1):93–102.
[64] Chen CS, Lin CY, Chien RD. Thermally induced buckling of functionally graded hybrid composite plates. Int J Mech Sci 2011;53(1):51–8.
[65] Ghannadpour SAM, Ovesy HR, Nassirnia M. Buckling analysis of functionally graded plates under thermal loadings using the finite strip method. Comput Struct 2012;108–109:93–9.
[66] Mansouri MH, Shariyat M. Thermal buckling predictions of three types of high-order theories for the heterogeneous orthotropic plates, using the new version of DQM. Compos Struct 2014;113:40–55.
[67] Fiorenzo AF. Natural frequencies and critical temperatures of functionally graded sandwich plates subjected to uniform and non-uniform temperature distributions. Compos Struct 2015;121:197–210.
[68] Carrera E. Transverse normal strain effects on thermal stress analysis of homogeneous and layered plates. AIAA J 2005;43(10):2232–42.
[69] Zhang LW, Zhu P, Liew KM. Thermal buckling of functionally graded plates using a local Kriging meshless method. Compos Struct 2014;108:472–92.
[70] Vuksanovic Dj. Linear analysis of laminated composite plates using single layer higher-order discrete models. Compos Struct 2000;48(3):205–11.
[71] Reddy JN. Mechanics of laminated composite plates. CRC Press; 2004.
[72] Fazzolari FA, Carrera E. Coupled thermoelastic effect in free vibration analysis of anisotropic multilayered plates and FGM plates by using a variable-kinematics Ritz formulation. Eur J Mech A Solids 2014;44:157–74.
[73] Brischetto S, Carrera E. Coupled thermo-mechanical analysis of one-layered and multilayered plates. Compos Struct 2010;92(8):1793–812.
[74] Brischetto S, Carrera E. Heat conduction and thermal analysis in multilayered plates and shells. Mech Res Commun 2011;38(6):449–55.
[75] Fazzolari FA, Carrera E. Free vibration analysis of sandwich plates with anisotropic face sheets in thermal environment by using the hierarchical trigonometric Ritz formulation. Compos B 2013;50:67–81.
[76] Giunta G, Crisafulli D, Belouettar S, Carrera E. A thermo-mechanical analysis of functionally graded beams via hierarchical modelling. Compos Struct 2013;95:676–90.
[77] Fazzolari FA. Natural frequencies and critical temperatures of functionally graded sandwich plates subjected to uniform and non-uniform temperature distributions. Compos Struct 2015;121:197–210.